



Centrum voor Wiskunde en Informatica

**REPORTRAPPORT**

Numerical Solution of Steady Free-Surface Navier-Stokes Flow

E.H. van Brummelen

Modelling, Analysis and Simulation (MAS)

**MAS-R0018 June 30, 2000**

Report MAS-R0018  
ISSN 1386-3703

CWI  
P.O. Box 94079  
1090 GB Amsterdam  
The Netherlands

CWI is the National Research Institute for Mathematics and Computer Science. CWI is part of the Stichting Mathematisch Centrum (SMC), the Dutch foundation for promotion of mathematics and computer science and their applications.

SMC is sponsored by the Netherlands Organization for Scientific Research (NWO). CWI is a member of ERCIM, the European Research Consortium for Informatics and Mathematics.

Copyright © Stichting Mathematisch Centrum  
P.O. Box 94079, 1090 GB Amsterdam (NL)  
Kruislaan 413, 1098 SJ Amsterdam (NL)  
Telephone +31 20 592 9333  
Telefax +31 20 592 4199

# Numerical Solution of Steady Free-Surface Navier-Stokes Flow

E.H. van Brummelen

CWI

P.O. Box 94079, 1090 GB Amsterdam, The Netherlands

## ABSTRACT

Numerical solution of flows that are partially bounded by a freely moving boundary is of great practical importance, e.g., in ship hydrodynamics. The usual time integration approach for solving steady viscous free surface flow problems has several drawbacks. Instead, we propose an efficient iterative method, which relies on a different but equivalent formulation of the free surface flow problem, involving a so-called quasi free-surface condition. It is shown that the method converges if the solution is sufficiently smooth in the neighborhood of the free surface. Details are provided for the implementation of the method in `parmax`. Furthermore, we present a method for analyzing properties of discretization schemes for the free-surface flow equations. Detailed numerical results are presented for flow over an obstacle in a channel. The results agree well with measurements as well as with the predictions of the analysis, and confirm that steady free-surface Navier-Stokes flow problems can indeed be solved efficiently with the new method.

*2000 Mathematics Subject Classification:* 35B20, 35R35, 65R20, 76D05, 76D33.

*Keywords and Phrases:* free-surface flows, incompressible Navier-Stokes equations, numerical solution methods, discrete dispersion relations.

*Note:* This work was performed under a research contract with the Maritime Research Institute Netherlands and was carried out under CWI-project MAS2.1 "Computational Fluid Dynamics".

## 1. INTRODUCTION

The numerical solution of flows that are partially bounded by a freely moving boundary is of great practical importance. The numerical techniques available to solve such free-surface flows, can be categorized into *surface tracking* methods, the most prominent being the marker and cell method [13] and the volume of fluid method [15], *interface capturing* methods, e.g., [17, 21], and *surface fitting* methods [9]. It is generally acknowledged that if the free-boundary is smooth, in particular if the surface can be represented by a so-called height function, surface fitting methods are unsurpassed in accuracy. Since the free-surfaces occurring in many practical applications, for instance, ship hydrodynamics, are smooth, surface fitting methods have received much attention.

If time-dependent surface fitting methods are considered, generally there is no essential difference in the treatment of the free-surface in potential flow or Navier-Stokes flow. Then, independent of the flow model, the solution of the flow equations and the geometry of the free-boundary are usually separated. The flow equations are integrated over a small time interval, with the dynamic conditions imposed at the free-surface. Subsequently, the position of the free surface is determined through the kinematic condition, employing the newly computed velocity field.

For surface fitting methods for steady free-surface flows, such a common approach for viscous and inviscid flows does not exist. Whereas dedicated techniques have been developed for steady potential flow [5, 6, 24], methods for Navier-Stokes flow simply continue the aforementioned transient process until a steady state is reached. In [23] several drawbacks of this process are discussed, such as slow convergence to steady state. In particular, from the results in [19] one infers that at subcritical Froude numbers, dispersion causes asymptotic temporal behavior of the amplitude of transient waves in  $\mathbb{R}^d$  of  $O(t^{-(d-1)/2})$ . Hence, if the objective is to reduce the amplitude of transient waves to the order

of spatial discretization errors, the efficiency of the time integration approach deteriorates rapidly with decreasing mesh-width. In practical computations, thousands of time steps are usually required, rendering the transient approach prohibitively expensive in actual design processes.

For efficiency, the methods developed for steady free-surface potential flow exploit the fact that during the solution process neither the kinematic nor the dynamic condition needs to be satisfied. Instead of imposing the dynamic condition on the sub-problems (i.e., the flow problems corresponding to a given free-surface position) and using the kinematic condition to determine a new approximation to the free-surface location, any combination of boundary conditions can be imposed on the sub-problems and any operator that locates the free surface can be employed, provided that the sub-problems are well-posed, the resulting iterative process converges and the converged solution satisfies both the dynamic and the steady kinematic conditions. This permits the construction of iterative algorithms that for each sub-problem evaluation provide a more accurate approximation to the steady free-surface position than would be obtained if the usual time-dependent approach were followed. Efforts can then be directed to solving the sub-problems efficiently.

To reduce the computational expense of solving the steady free-surface flow problem, we propose an efficient iterative solution method. The method relies on a different but equivalent formulation of the free-surface flow problem, involving a so-called quasi free-surface condition [4]. The method solves a sequence of steady Navier-Stokes sub-problems with this condition imposed at an approximation to the steady free boundary. After each sub-problem evaluation, the free surface is displaced. Due to the choice of the boundary conditions at the free surface, each sub-problem evaluation yields an improved approximation to the steady free-surface position. Considering the free-surface flow problem as an optimal shape design problem, we will show that the iterative method results in the minimization of a cost functional subject to a constraint, provided that the flow is sufficiently smooth. Convergence of the method is then ensured.

To improve the accuracy of numerical results, a priori knowledge of the properties of the discretization scheme is indispensable. We present a method for analyzing the properties of the discretized equations corresponding to the sub-problems. The analysis yields valuable information on the effects of discretization errors on the numerical results. Inversely, it can serve in the development of discretization schemes with favorable properties, e.g., low numerical damping of gravity waves.

Implementation of the iterative method in `parmax` [16] is realized and numerical results are presented for the flow over a protuberance in a channel of unit depth.

## 2. INCOMPRESSIBLE FREE-SURFACE FLOW

In this section we state the equations governing incompressible free-surface flow. First, we briefly discuss the equations describing viscous flow. Subsequently, appropriate interface conditions for free surface flows are given and the quasi free-surface condition is introduced.

### 2.1 Substrate

As the substrate of the free surface, we consider an incompressible, viscous fluid flow, subject to a constant gravitational force on a time-dependent spatial domain,  $\mathcal{V}(t)$ . The domain is bounded by a moving boundary,  $\mathcal{S}(t)$ , and fixed boundaries  $\partial\mathcal{V}\setminus\mathcal{S}$ . The flow is characterized by the Froude number,  $Fr$ , and the Reynolds number,  $Re$ . Although we are interested in steady solutions only, for the purpose of analysis we consider the equations describing the aforementioned flow in their time-dependent form. The (non-dimensionalized) fluid velocity and pressure are identified by  $\mathbf{v}(\mathbf{x}, t)$  and  $p(\mathbf{x}, t)$ , respectively, with  $t \geq 0$  and  $\mathbf{x} = x_\alpha \mathbf{e}^{(\alpha)} \in \mathbb{R}^d$  ( $d = 2, 3$ ). Here  $\mathbf{e}^{(\alpha)}$  and  $x_\alpha$  denote Cartesian base vectors and coordinates, respectively, and the summation convention applies to paired super- and subscripts, unless mentioned otherwise. Further, assuming the gravitational force to act in the negative (vertical)  $x_d$ -direction, it proves useful to introduce the hydrodynamic pressure,  $\varphi(\mathbf{x}, t) \equiv p(\mathbf{x}, t) + Fr^{-2}x_d$ . Incompressibility of the fluid implies that the velocity field is solenoidal:

$$M(\mathbf{v}, \varphi) \equiv \operatorname{div} \mathbf{v} = 0, \quad \mathbf{x} \in \mathcal{V}(t), t > 0. \quad (2.1a)$$

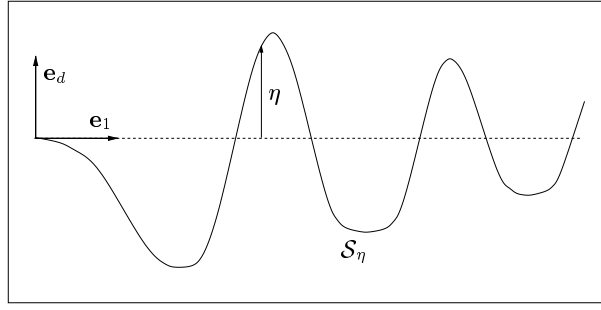


Figure 1: schematic illustration of the free-surface problem.

Conservation of momentum is expressed by

$$\mathbf{N}(\mathbf{v}, \varphi) \equiv \frac{\partial \mathbf{v}}{\partial t} + \operatorname{div} \mathbf{v} \mathbf{v} + \nabla \varphi - \operatorname{div} \boldsymbol{\tau}(\mathbf{v}) = 0, \quad \mathbf{x} \in \mathcal{V}(t), t > 0, \quad (2.1b)$$

where  $\boldsymbol{\tau}(\mathbf{v})$  is the viscous stress tensor for a Newtonian fluid, with Cartesian components

$$\tau_{\alpha\beta}(\mathbf{v}) = \operatorname{Re}^{-1} \left( \frac{\partial v_\beta}{\partial x_\alpha} + \frac{\partial v_\alpha}{\partial x_\beta} - \lambda (\nabla \cdot \mathbf{v}) \delta_{\alpha\beta} \right). \quad (2.1c)$$

Here  $\delta_{\alpha\beta}$  is the Kronecker symbol and  $\lambda$  is Stokes' constant. Clearly, for a solenoidal velocity field, the part multiplied by  $\lambda$  vanishes. Moreover, if the Reynolds number is spatially invariant, the viscous term reduces to

$$\operatorname{div} \boldsymbol{\tau}(\mathbf{v}) = \operatorname{Re}^{-1} \Delta \mathbf{v}. \quad (2.2)$$

## 2.2 Free-surface conditions

Free-surface flows are essentially two-phase flows, of which the properties of the contiguous bulk-fluids are such that their mutual interaction at the interface can be ignored. For an elaborate discussion of two-phase flows, see, for example, [1] and [26]. The free-surface conditions follow from the general interface conditions and the assumptions that both density and viscosity of the adjacent fluid vanish at the interface and, furthermore, that the interface is impermeable. Moreover, here it will be assumed that interfacial stresses can be ignored, which is a valid assumption in many practical applications.

Let  $\mathcal{S}_0$  denote a reference surface, e.g., the undisturbed interface. We consider interfaces that can be represented as  $\mathcal{S}_\eta = \{\mathbf{x} + \eta(\mathbf{x}_-, t) \mathbf{e}_d \mid \mathbf{x} \in \mathcal{S}_0\}$ , where  $\mathbf{x}_- = (x_1, \dots, x_{d-1})$  and the vertical distance from the free surface to the reference surface,  $\eta(\mathbf{x}_-, t)$ , is assumed to be a sufficiently regular function; see the illustration in Figure 1. The motion of the free surface is governed by a kinematic condition and  $d$  dynamic conditions. Impermeability dictates that a fluid particle is confined to the free surface:

$$\frac{Dx_d}{Dt} - \frac{D\eta(\mathbf{x}_-, t)}{Dt} = 0, \quad \mathbf{x} \in \mathcal{S}_\eta, t \geq 0,$$

where  $D/Dt$  is the total derivative. This translates into the kinematic condition

$$K(\mathbf{v}, \eta) \equiv \frac{\partial \eta}{\partial t} + \mathbf{v} \cdot \nabla (\eta - x_d) = 0, \quad \mathbf{x} \in \mathcal{S}_\eta, t \geq 0. \quad (2.3a)$$

Continuity of stresses at the interface is expressed by the normal dynamic condition  $p = 0$ , or, equivalently,

$$N(\varphi, \eta) \equiv \varphi - \operatorname{Fr}^{-2} \eta = 0, \quad \mathbf{x} \in \mathcal{S}_\eta, t \geq 0, \quad (2.3b)$$

and  $d - 1$  tangential dynamic conditions

$$T^\alpha(\mathbf{v}, \eta) \equiv \mathbf{t}^\alpha \cdot \boldsymbol{\tau}(\mathbf{v}) \cdot \mathbf{n} = 0, \quad \mathbf{x} \in \mathcal{S}_\eta, t \geq 0. \quad (2.3c)$$

Here,  $\mathbf{t}^\alpha$  ( $\alpha = 1, \dots, d - 1$ ) are orthogonal unit tangent vectors to  $\mathcal{S}_\eta$  and  $\mathbf{n}$  denotes the unit normal vector to  $\mathcal{S}_\eta$ . Notice that (2.3b) implies that the non-dimensionalized pressure vanishes at the free surface. Hence, assuming that viscous contributions to the normal stress are negligible, which is generally appropriate because  $\mathbf{n} \cdot \boldsymbol{\tau}(\mathbf{v}) \cdot \mathbf{n}$  is small in the neighborhood of the free surface, the combined free-surface conditions, (2.3), imply that there is no transfer of either mass or momentum through the free-surface. Furthermore note that (2.3c) is naturally satisfied for inviscid fluids. Therefore, equations (2.3c) are often referred to as viscous free-surface conditions.

### 2.3 Quasi free-surface condition

Free-boundary problems generally permit many equivalent formulations. However, although these formulations are equivalent, their suitability for numerical simulation can differ significantly. Efficient numerical solution of steady free-boundary problems demands that an accurate approximation to the solution can be computed on a fixed domain. To this end, a condition that holds on a boundary in the neighborhood of the actual free boundary is required. We refer to such a condition as a *quasi free-surface condition*, because the qualitative solution behavior of the corresponding (initial) boundary value problem is similar to that of the free boundary problem, but the boundary does not actually move. Below, we derive a suitable quasi free-surface condition for the free-surface Navier-Stokes problem.

Let  $\mathcal{S}_0$  designate the undisturbed free surface. We introduce a nearby, fixed boundary by displacing  $\mathcal{S}_0$  along the vertical unit vector:

$$\mathcal{S}_{\epsilon\bar{\eta}} = \{\mathbf{x} + \epsilon\bar{\eta}(\mathbf{x}_-) \mathbf{e}_d \mid \mathbf{x} \in \mathcal{S}_0\}, \quad (2.4)$$

where  $\bar{\eta}(\mathbf{x}_-)$  stands for a sufficiently regular function, independent of  $\epsilon$ . Likewise,  $\mathcal{S}_{\epsilon\eta}$  represents the actual free surface, which we also assume to be located at an  $O(\epsilon)$ -distance from  $\mathcal{S}_0$ . We suppose that  $p(\mathbf{x}, t)$  and  $\mathbf{v}(\mathbf{x}, t)$  can be extended smoothly beyond the boundary  $\mathcal{S}_{\epsilon\bar{\eta}}$ . Taylor expansion in the neighborhood of  $\mathcal{S}_{\epsilon\bar{\eta}}$  then yields for  $p(\mathbf{x}, t)$  and  $\mathbf{v}(\mathbf{x}, t)$  at the actual free surface,

$$p(\mathbf{x} + \epsilon(\eta(\mathbf{x}_-, t) - \bar{\eta}(\mathbf{x}_-)) \mathbf{e}_d, t) = p(\mathbf{x}, t) + \epsilon(\eta(\mathbf{x}_-, t) - \bar{\eta}(\mathbf{x}_-)) \mathbf{e}_d \cdot \nabla p(\mathbf{x}, t) + O(\epsilon^2), \quad (2.5a)$$

$$\mathbf{v}(\mathbf{x} + \epsilon(\eta(\mathbf{x}_-, t) - \bar{\eta}(\mathbf{x}_-)) \mathbf{e}_d, t) = \mathbf{v}(\mathbf{x}, t) + \epsilon(\eta(\mathbf{x}_-, t) - \bar{\eta}(\mathbf{x}_-)) \mathbf{e}_d \cdot \nabla \mathbf{v}(\mathbf{x}, t) + O(\epsilon^2), \quad (2.5b)$$

for  $\mathbf{x} \in \mathcal{S}_{\epsilon\bar{\eta}}$ . By the dynamic condition, (2.3b), the lefthand side of (2.5a) vanishes, and the displacement of the free-surface is estimated

$$\epsilon\eta(\mathbf{x}_-, t) = \frac{-p(\mathbf{x}, t)}{\mathbf{e}_d \cdot \nabla p(\mathbf{x}, t)} + \epsilon\bar{\eta}(\mathbf{x}_-) + O(\epsilon^2), \quad \mathbf{x} \in \mathcal{S}_{\epsilon\bar{\eta}}. \quad (2.6)$$

We assume that  $p(\mathbf{x}, t)$  is smooth in  $x_d$ , in such a manner that the vertical component of the pressure gradient is dominated by the hydrostatic component, specifically,  $\mathbf{e}_d \cdot \nabla p = -\text{Fr}^{-2} + O(\epsilon)$ . Notice that (2.5a) and the dynamic condition (2.3b) imply that  $p(\mathbf{x}, t) = O(\epsilon)$  for  $\mathbf{x} \in \mathcal{S}_{\epsilon\theta}$ . Hence,

$$\epsilon\eta(\mathbf{x}_-, t) = \text{Fr}^2 p(\mathbf{x}, t) + \epsilon\bar{\eta}(\mathbf{x}_-) + O(\epsilon^2) = \text{Fr}^2 \varphi(\mathbf{x}, t) + O(\epsilon^2). \quad (2.7)$$

Inserting this approximation of  $\epsilon\eta(\mathbf{x}_-, t)$  into the kinematic condition (2.3a) and applying (2.5b), one obtains

$$\frac{\partial \varphi}{\partial t} + \mathbf{v} \cdot \nabla (\varphi - \text{Fr}^{-2} x_d) = -\epsilon(\eta - \bar{\eta}) \mathbf{e}_d \cdot \nabla \mathbf{v} \cdot \nabla (\varphi - \text{Fr}^{-2} x_d) + O(\epsilon^2). \quad (2.8)$$

Assuming that in the neighborhood of  $\mathcal{S}_{\epsilon\eta}$ ,  $\mathbf{v}(\mathbf{x}, t)$  is smooth in  $x_d$ , in particular,  $\mathbf{e}_d \cdot \nabla \mathbf{v} = O(\epsilon)$ , the righthand side of (2.8) is of  $O(\epsilon^2)$ . Hence, summarizing, if the free-surface conditions (2.3a) and

(2.3b), hold at the actual free surface,  $\mathcal{S}_{\epsilon\eta}$ , at an  $O(\epsilon)$ -distance from the undisturbed free surface, and if  $p(\mathbf{x}, t)$  and  $\mathbf{v}(\mathbf{x}, t)$  are sufficiently smooth in  $x_d$  in the neighborhood of the free surface, then the quasi free-surface condition,

$$K(\mathbf{v}, \text{Fr}^2\varphi) = 0, \quad \mathbf{x} \in \mathcal{S}_{\epsilon\bar{\eta}}, \quad (2.9)$$

with  $K$  according to (2.3a), approximates to  $O(\epsilon^2)$  the conditions at the fixed boundary  $\mathcal{S}_{\epsilon\bar{\eta}}$ , also located at an  $O(\epsilon)$ -distance from the undisturbed free surface. Therefore, conversely, if (2.9) is imposed at the fixed boundary  $\mathcal{S}_{\epsilon\bar{\eta}}$ , then the solution complies to  $O(\epsilon^2)$  with the kinematic condition (2.3a) and the dynamic condition (2.3b) at  $\mathcal{S}_{\epsilon\eta}$ . Consequently, the initial boundary value problem that is associated with the incompressible Navier-Stokes equations with the quasi free-surface condition imposed on  $\mathcal{S}_{\epsilon\bar{\eta}}$  displays similar behavior as the corresponding free-boundary problem. Moreover, by (2.6), the position of the actual free boundary can be estimated

$$\mathcal{S}_{\epsilon\eta} = \{\mathbf{x} + \text{Fr}^2\varphi(\mathbf{x}, t) \mathbf{e}_d \mid \mathbf{x} \in \mathcal{S}_0\}, \quad (2.10)$$

with  $\varphi(\mathbf{x}, t)$  the solution of the initial boundary value problem.

An iterative method for solving the steady free-surface Navier-Stokes problem based on (2.9) and (2.10) can now be constructed in the following manner: For a given estimation of the position of the free surface, one solves the steady Navier-Stokes equations, subject to the steady quasi free-surface condition and the viscous dynamic conditions at the estimated free surface, and appropriate boundary conditions at fixed boundaries. Next, the free surface is displaced according to equation (2.10), to obtain an improved approximation to the free surface position, and the process is repeated.

### 3. OPTIMAL SHAPE DESIGN FORMULATION

Free-boundary problems are closely related to constrained shape optimization problems. A general characteristic of free boundary problems is that the number of free-boundary conditions is one more than the number of boundary conditions required by the boundary value problem. Therefore, if a cost functional is defined to be some norm of the residual of any of the free-boundary conditions, then minimizing this cost functional, subject to the boundary value problem with the remaining free-boundary conditions imposed at the free boundary, yields the desired solution of the free-boundary problem. In this section we will further explore this analogy.

#### 3.1 Problem statement

Let  $\mathcal{O}$  denote the space of admissible domains for the free-surface flow problems. A detailed discussion on admissibility criteria for domains for optimal shape design, for problems governed by elliptic differential equations, can be found in [22]. An optimal shape design problem corresponding to the steady free-surface flow problem reads:

$$\min_{\mathcal{V} \in \mathcal{O}} \int_{\mathcal{S}} |p(\mathbf{x})| \, d\mathcal{S} \quad (3.1)$$

subject to the constraint  $\mathcal{C}(\mathcal{V}, \mathbf{v}, p)$ :

$$\left. \begin{aligned} \text{div } \mathbf{v}\mathbf{v} + \nabla p - \text{div } \boldsymbol{\tau}(\mathbf{v}) &= -\text{Fr}^{-2} \mathbf{e}_d \\ \text{div } \mathbf{v} &= 0 \end{aligned} \right\}, \quad \mathbf{x} \in \mathcal{V}, \quad (3.2a)$$

$$\mathbf{B}(\mathbf{v}, p) = \mathbf{b}(\mathbf{x}), \quad \mathbf{x} \in \partial\mathcal{V} \setminus \mathcal{S}, \quad (3.2b)$$

$$\left. \begin{aligned} \mathbf{t}^\alpha \cdot \boldsymbol{\tau}(\mathbf{v}) \cdot \mathbf{n} &= 0 \\ \mathbf{v} \cdot \nabla p &= 0 \end{aligned} \right\}, \quad \mathbf{x} \in \mathcal{S}, \quad (3.2c)$$

with  $\alpha = 1, \dots, d-1$ . Here, equation (3.2b) stands for boundary conditions on the fixed boundaries. Equation (3.1) shows the cost functional, and the domain  $\mathcal{V}$  is referred to as the *design variable*. If the

domain  $\mathcal{V}$  can be parameterized, then the parameters are also called design variables. In particular, if the free-boundary can be represented by a height function, the height function is the design variable.

Obviously, many equivalent formulations exist. For instance, the second boundary condition in (3.2c) can be replaced by

$$\mathbf{v}(\mathbf{x}) \cdot \mathbf{n}(\mathbf{x}) = 0, \quad \mathbf{x} \in \mathcal{S}. \quad (3.3)$$

Alternatively, the cost functional can be modified, e.g.,

$$\min_{\mathcal{V} \in \mathcal{O}} \int_{\mathcal{S}} (\mathbf{v}(\mathbf{x}) \cdot \mathbf{n}(\mathbf{x}))^2 d\mathcal{S}. \quad (3.4)$$

However, although these formulations are equivalent, the complexity of the optimization problem can depend sensitively on the formulation; see [27]. Our choice for formulation (3.1), (3.2) is motivated below.

### 3.2 Descent methods

Suppose that the objective is to minimize the functional

$$E(\mathcal{S}, \mathbf{q}) = \int_{\mathcal{S}} L(\mathbf{q}) d\mathcal{S}, \quad (3.5)$$

over all  $\mathcal{V} \in \mathcal{O} \subset \mathbb{R}^d$ , subject to the constraint  $\mathcal{C}(\mathcal{V}, \mathbf{q})$ , where  $\mathcal{S} \subseteq \partial\mathcal{V}$  and where  $L$  stands for an appropriate operator. Moreover, suppose that the problem has a unique solution. Following [22], we assume that  $\mathcal{V}$  is sufficiently regular, so that for a suitable function  $\alpha(\mathbf{x})$  on  $\mathcal{S}$ ,

$$\mathcal{S}_{\epsilon\alpha} = \{\mathbf{x} + \epsilon\alpha(\mathbf{x})\mathbf{n}(\mathbf{x}) \mid \mathbf{x} \in \mathcal{S}\} \quad (3.6)$$

is the boundary of a domain  $\mathcal{V}_{\epsilon\alpha}$  close to  $\mathcal{V}$ . Thus, we obtain  $\mathcal{V}_{\epsilon\alpha}$  from  $\mathcal{V}$  by displacing the boundary along its normal. We imagine  $\mathcal{V}$  and  $\mathcal{V}_{\epsilon\alpha}$  to be embedded in a larger domain,  $\mathcal{E}$ , and we suppose that for all  $\mathcal{V} \subset \mathcal{E}$  a solution  $\mathbf{q}(\mathbf{x})$  of the constraint  $\mathcal{C}(\mathcal{V}, \mathbf{q})$  extends smoothly beyond the boundary  $\partial\mathcal{V}$ , so that  $\mathbf{q}(\mathbf{x})$  is well defined for all  $\mathbf{x} \in \mathcal{E}$ . In [22, pp.81–91] it is proved that for  $\epsilon \rightarrow 0$ ,

$$\frac{1}{\epsilon} (E(\mathcal{S}_{\epsilon\alpha}, \mathbf{q}_{\epsilon\alpha}) - E(\mathcal{S}, \mathbf{q})) \sim \int_{\mathcal{S}} \left( -\alpha(\mathbf{x}) \frac{L(\mathbf{q})}{R(\mathbf{x})} + L'(\mathbf{q}) (\alpha(\mathbf{x}) \mathbf{n}(\mathbf{x}) \cdot \nabla \mathbf{q}(\mathbf{x}) + \mathbf{q}'_{\alpha}(\mathbf{x})) \right) d\mathcal{S}, \quad (3.7)$$

where  $\mathbf{q}_{\epsilon\alpha}$  follows from the constraint  $\mathcal{C}(\mathcal{V}_{\epsilon\alpha}, \mathbf{q}_{\epsilon\alpha})$  and  $\mathbf{q}'_{\alpha}(\mathbf{x})$  is defined by

$$\mathbf{q}_{\epsilon\alpha}(\mathbf{x}) = \mathbf{q}(\mathbf{x}) + \epsilon \mathbf{q}'_{\alpha}(\mathbf{x}) + O(\epsilon^2), \quad \text{for } \epsilon \rightarrow 0. \quad (3.8)$$

Hence,  $\epsilon \mathbf{q}'_{\alpha}(\mathbf{x})$  is the disturbance in the solution of the constraint, induced by the displacement of the boundary and the corresponding change in the shape of the domain. Alternatively,  $\epsilon \mathbf{q}'_{\alpha}(\mathbf{x})$  can be regarded as the projection on  $\mathcal{V}_{\epsilon\alpha} - \mathcal{V}$  of the gradient of  $\mathbf{q}(\mathbf{x})$  with respect to  $\mathcal{V}$ . The derivative  $L'(\mathbf{q})$  is defined by

$$L(\mathbf{q} + \epsilon \mathbf{q}') = L(\mathbf{q}) + \epsilon L'(\mathbf{q}) \mathbf{q}' + O(\epsilon^2), \quad \text{for } \epsilon \rightarrow 0, \quad (3.9)$$

for all suitable functions  $\mathbf{q}'(\mathbf{x})$ . Furthermore,  $R(\mathbf{x})$  denotes the radius of curvature of  $\mathcal{S}$  if  $d = 2$  and the mean radius of curvature if  $d = 3$ . In the case that the argument of the integral (3.7) does not exist at a finite number of isolated points on  $\mathcal{S}$ , these points are replaced by appropriate limits.

If  $\alpha(\mathbf{x})$  is chosen such that the right-hand side of (3.7) is negative, a modification of the domain such that the boundary changes from  $\mathcal{S}$  to  $\mathcal{S}_{\epsilon\alpha}$  according to (3.6), with  $\epsilon$  a small positive number, results in a reduction of the cost functional. Such a choice for  $\alpha(\mathbf{x})$  is referred to as a descent direction. We call  $\epsilon$  the step-size and  $\epsilon\alpha(\mathbf{x})$  the correction. A (local) minimum of the cost functional can thus be

obtained by repeatedly modifying the design variable in a descent direction. A method based on this principle is called a descent method. A minimum is attained if the right-hand side of (3.7) is positive definite for all allowable  $\alpha(\mathbf{x})$ , i.e., if there exists no  $\alpha(\mathbf{x})$  that yields a further reduction of the cost functional. We require that the corrections vanish when the cost functional approaches its minimum, thus ensuring that the minimum is a fixed point of the descent method.

The difficulty in determining a descent direction from (3.7) is its dependence on the induced disturbance,  $\mathbf{q}'_\alpha(\mathbf{x})$ , which is connected to  $\alpha(\mathbf{x})$  through the constraint,  $\mathcal{C}(\mathcal{V}, \mathbf{q})$ . In [28] the dependence of the variation of the functional on  $\mathbf{q}'_\alpha(\mathbf{x})$  is eliminated by choosing a suitable descent direction. To determine this descent direction, an adjoint problem is solved. This approach is general, but the formulation and solution of the adjoint problem can be intricate.

### 3.3 Quasi implicit boundary conditions

In specific cases, the dependence of the variation of the cost functional on  $\mathbf{q}'_\alpha(\mathbf{x})$  can also be eliminated by a proper formulation of the constraint. In the case that the constraint consists of a boundary value problem, the difference in formulations involves the boundary conditions and the cost functional only. Next, we construct equivalent boundary conditions with the property that a modification of the domain from  $\mathcal{V}$  to  $\mathcal{V}_{\epsilon\alpha}$  introduces a relative induced disturbance,

$$\frac{\mathbf{q}'_\alpha(\mathbf{x})}{\alpha(\mathbf{x})} = O(\epsilon), \quad \mathbf{x} \in \mathcal{S}. \quad (3.10)$$

This implies that if  $\mathcal{V}$  is a domain at an  $O(\epsilon)$ -distance from the optimal domain and  $\mathbf{q}(\mathbf{x})$  is the associated solution of the constraint, and for some suitable  $\alpha(\mathbf{x})$ ,  $\mathcal{V}_{\epsilon\alpha}$  according to (3.6) is the optimal domain with associated solution  $\mathbf{q}_{\epsilon\alpha}(\mathbf{x})$ , then  $\|\mathbf{q}_{\epsilon\alpha} - \mathbf{q}\|_{\mathcal{E}} = O(\epsilon^2)$ . Because the solution  $\mathbf{q}(\mathbf{x})$  satisfies to  $O(\epsilon^2)$  the actual free-boundary conditions at the modified free-boundary position,  $\mathcal{S}_{\epsilon\alpha}$ , we call such a boundary condition *quasi implicit*. Thus, if the constraint with the quasi implicit boundary condition imposed at the free-boundary is solved on  $\mathcal{V}$  and, subsequently, the domain is modified to  $\mathcal{V}_{\epsilon\alpha}$  and the constraint with the original boundary condition imposed at the modified free-boundary is solved, then the incurred disturbance is  $O(\epsilon^2)$  and can be ignored. Then, by (3.7), an allowable  $\alpha(\mathbf{x})$  that satisfies

$$-\alpha(\mathbf{x}) \frac{L(\mathbf{q})}{R(\mathbf{x})} + L'(\mathbf{q})(\alpha(\mathbf{x}) \mathbf{n}(\mathbf{x}) \cdot \nabla \mathbf{q}(\mathbf{x})) < 0, \quad \mathbf{x} \in \mathcal{S}, \quad (3.11)$$

is a descent direction. Note that by (3.11),

$$\alpha(\mathbf{x}) = \frac{L(\mathbf{q})}{R(\mathbf{x})} - L'(\mathbf{q}) \mathbf{n}(\mathbf{x}) \cdot \nabla \mathbf{q}(\mathbf{x}) \quad \mathbf{x} \in \mathcal{S}, \quad (3.12)$$

specifies a descent direction. Thus, one can express a descent direction explicitly in  $\mathcal{S}$ , through its normal vector and curvature, and in the solution of the constraint with the quasi implicit boundary condition imposed at  $\mathcal{S}$ . One may note that, due to the disappearance of the induced disturbance, the determination of a descent direction is disconnected from the constraint and, therefore, it is essentially the same as determining a descent direction in the case of unconstrained optimization.

We denote the boundary conditions at the free-boundary,  $\mathcal{S}$ , as specified by the constraint,  $\mathcal{C}(\mathcal{V}, \mathbf{q})$ , by

$$\mathbf{S}(\mathcal{S}, \mathbf{q}(\mathbf{x})) = 0, \quad \mathbf{x} \in \mathcal{S}, \quad (3.13)$$

for a suitable operator  $\mathbf{S}$ . The boundary conditions can depend explicitly on  $\mathcal{S}$ , for instance, through its normal vector. Let  $\mathcal{S}$  denote a boundary at an  $O(\epsilon)$ -distance from the actual free boundary. Let  $\alpha(\mathbf{x})$  be a descent direction for the cost functional under the assumption that the induced disturbance is negligible, i.e., compliant with (3.11). The aim is to derive a boundary condition on  $\mathcal{S}$  with

the property that a solution of the corresponding constraint obeys to  $O(\epsilon^2)$  the original boundary condition (3.13) at the modified boundary,  $\mathcal{S}_{\epsilon\alpha}$ . Then, conversely, if the domain is changed from  $\mathcal{V}$  to  $\mathcal{V}_{\epsilon\alpha}$  and the original boundary condition is imposed on  $\mathcal{S}_{\epsilon\alpha}$ , the relative induced disturbance is of  $O(\epsilon)$  and the induced disturbance is indeed negligible, so that the initial assumption holds.

Let  $\mathcal{S}$  stand for an approximation to the free-boundary, at an  $O(\epsilon)$ -distance from the optimal free-boundary position. We introduce a nearby boundary,  $\mathcal{S}_{\epsilon\alpha}$ , obtained from  $\mathcal{S}$  according to (3.6), for some suitable  $\alpha(\mathbf{x})$ . The corresponding solution of the constraint is denoted by  $\mathbf{q}_{\epsilon\alpha}(\mathbf{x})$ , i.e.,  $\mathcal{C}(\mathcal{V}_{\epsilon\alpha}, \mathbf{q}_{\epsilon\alpha})$ . The boundary conditions (3.13) can be transferred from  $\mathcal{S}_{\epsilon\alpha}$  to  $\mathcal{S}$ :

$$\mathbf{S}(\mathcal{S}_{\epsilon\alpha}, \mathbf{q}_{\epsilon\alpha}(\mathbf{x} + \epsilon\alpha(\mathbf{x})\mathbf{n}(\mathbf{x}))) = 0, \quad \mathbf{x} \in \mathcal{S}. \quad (3.14)$$

Hence, equation (3.14) specifies the conditions at  $\mathcal{S}$  if the boundary conditions are satisfied at  $\mathcal{S}_{\epsilon\alpha}$ . Assuming that  $\mathbf{q}_{\epsilon\alpha}(\mathbf{x})$  is well defined beyond the boundary  $\mathcal{S}_{\epsilon\alpha}$  and continuously differentiable in the neighborhood of  $\mathcal{S}$ , Taylor expansion yields

$$\mathbf{q}_{\epsilon\alpha}(\mathbf{x} + \epsilon\alpha(\mathbf{x})\mathbf{n}(\mathbf{x})) = \mathbf{q}_{\epsilon\alpha}(\mathbf{x}) + \epsilon\alpha(\mathbf{x})\mathbf{n}(\mathbf{x}) \cdot \nabla \mathbf{q}_{\epsilon\alpha}(\mathbf{x}) + O(\epsilon^2), \quad \mathbf{x} \in \mathcal{S}. \quad (3.15)$$

From (3.14) and (3.15) it follows that if we introduce a modified constraint,  $\mathcal{C}_{\epsilon\alpha}(\mathcal{V}, \mathbf{q})$ , similar to the original constraint, but with the boundary condition (3.13) replaced by

$$\mathbf{S}(\mathcal{S}_{\epsilon\alpha}, \mathbf{q}(\mathbf{x}) + \epsilon\alpha(\mathbf{x})\mathbf{n}(\mathbf{x}) \cdot \nabla \mathbf{q}(\mathbf{x})) = 0, \quad \mathbf{x} \in \mathcal{S}, \quad (3.16)$$

that the relative difference between the solution to the modified constraint and the solution to the original constraint at  $\mathcal{S}$  is  $O(\epsilon)$ , i.e., if  $\mathcal{V}, \mathbf{q}$  obey  $\mathcal{C}_{\epsilon\alpha}(\mathcal{V}, \mathbf{q})$  and  $\mathcal{V}_{\epsilon\alpha}, \mathbf{q}_{\epsilon\alpha}$  obey  $\mathcal{C}(\mathcal{V}_{\epsilon\alpha}, \mathbf{q}_{\epsilon\alpha})$ , then the relative difference at  $\mathcal{S}$  satisfies

$$\frac{\mathbf{q}_{\epsilon\alpha}(\mathbf{x}) - \mathbf{q}(\mathbf{x})}{\epsilon\alpha(\mathbf{x})} = O(\epsilon), \quad \mathbf{x} \in \mathcal{S}. \quad (3.17)$$

Hence, if the modified constraint is solved on  $\mathcal{V}$  and, subsequently, the domain is changed to  $\mathcal{V}_{\epsilon\alpha}$  and the original constraint is solved on  $\mathcal{V}_{\epsilon\alpha}$ , then the relative induced disturbance fulfills (3.10). Moreover, condition (3.16) reduces to (3.13) if  $\mathcal{S}$  is the optimal free boundary, because the correction  $\epsilon\alpha(\mathbf{x})$  vanish. Condition (3.16) and (3.13) are thus equivalent and (3.16) is a quasi implicit boundary condition.

We already remarked that many equivalent formulations of the optimal shape design problem exist. One should anticipate that posedness of the modified constraint, i.e., the boundary value problem associated with (3.16), depends on the choice of the boundary condition (3.13).

Summarizing, one can determine a descent direction,  $\alpha(\mathbf{x})$ , from (3.11) under the assumption that the induced disturbance is negligible. Then, once a step size  $\epsilon > 0$  has been decided, the corresponding quasi implicit boundary conditions can be obtained from (3.16). Next, the modified constraint, i.e., the boundary value problem associated with the quasi implicit boundary condition, is solved and the boundary is relocated according to (3.6). Because the quasi implicit boundary condition ensures that the induced disturbance is indeed negligible, the initial assumption holds, and  $\mathcal{S}_{\epsilon\alpha}$  improves  $\mathcal{S}$ . Moreover, due to the equivalence of the quasi implicit boundary condition and the original boundary condition, the modified constraint tends to the original constraint as  $\mathcal{S}$  approaches the optimal free boundary position.

In practice, it will usually not be necessary to impose (3.16) exactly. For convergence to the optimal solution, it is sufficient that the boundary conditions are equivalent and that the relative induced disturbance is sufficiently small to ensure that the assumption that a descent direction can be determined from (3.11) is not violated.

### 3.4 Application to free-surface flow

We return to the optimal shape design problem corresponding to the free-surface flow problem, with cost functional (3.1) and constraint (3.2). Upon applying (3.7) to the cost functional in (3.1), one

obtains for  $\epsilon \rightarrow 0$ ,

$$\begin{aligned} \frac{1}{\epsilon} \left( \int_{\mathcal{S}_{\epsilon\alpha}} |p_{\epsilon\alpha}(\mathbf{x})| d\mathcal{S}_{\epsilon\alpha} - \int_{\mathcal{S}} |p(\mathbf{x})| d\mathcal{S} \right) &= \int_{\mathcal{S}} -\alpha(\mathbf{x}) \frac{|p(\mathbf{x})|}{R(\mathbf{x})} d\mathcal{S} \\ &+ \int_{\mathcal{S}} \text{sign}(p(\mathbf{x})) \alpha(\mathbf{x}) \mathbf{n}(\mathbf{x}) \cdot \nabla p(\mathbf{x}) d\mathcal{S} + \int_{\mathcal{S}} \text{sign}(p(\mathbf{x})) p'_\alpha d\mathcal{S} + O(\epsilon). \end{aligned} \quad (3.18)$$

If  $\mathcal{S}$  is sufficiently smooth to neglect the first integral on the right-hand side of (3.18) and the relative induced disturbance is indeed negligible, then a descent direction is an allowable  $\alpha(\mathbf{x})$  for which

$$\text{sign}(p(\mathbf{x})) \alpha(\mathbf{x}) \mathbf{n}(\mathbf{x}) \cdot \nabla p(\mathbf{x}) < 0. \quad (3.19)$$

More precisely, rearranging (3.18), one finds that the descent step

$$\epsilon\alpha(\mathbf{x}) = \frac{-p(\mathbf{x})}{\mathbf{n}(\mathbf{x}) \cdot \nabla p(\mathbf{x})} \quad (3.20)$$

reduces the cost functional at  $\mathcal{S}_{\epsilon\alpha}$  most effectively. Notice that  $\epsilon\alpha(\mathbf{x})$  vanishes indeed when the cost functional approaches its minimum, i.e., when  $p(\mathbf{x})$  vanishes.

Instead of displacing the free-boundary along its normal, it is usually more convenient to displace it vertically. Equation (3.20) for the descent step is then replaced by

$$\epsilon\delta(\mathbf{x}) = \frac{-p(\mathbf{x})}{\mathbf{e}_d \cdot \nabla p(\mathbf{x})}, \quad (3.21)$$

with  $\epsilon\delta(\mathbf{x}) \mathbf{e}_d$  the vertical displacement of the boundary. If  $p(\mathbf{x})$  is smooth in  $x_d$ , then the vertical component of the pressure gradient is dominated by the hydrostatic component, i.e., we can estimate  $\mathbf{e}_d \cdot \nabla p(\mathbf{x}) \approx -\text{Fr}^{-2}$ . Thus we obtain

$$\tilde{\epsilon}\delta(\mathbf{x}) = \text{Fr}^2 p(\mathbf{x}), \quad (3.22)$$

as an approximation to the optimal descent step in case  $p(\mathbf{x})$  is smooth in  $x_d$  at  $\mathcal{S}$ .

The boundary conditions at the free boundary as specified by the constraint are given by (3.2c). Next, we derive the corresponding quasi implicit boundary condition, i.e., the conditions to  $O(\epsilon^2)$  at  $\mathcal{S}$  if (3.2c) applies at  $\mathcal{S}_{\epsilon\delta} = \{\mathbf{x} + \epsilon\delta(\mathbf{x}) \mathbf{e}_d \mid \mathbf{x} \in \mathcal{S}\}$ . Denoting the tangential and normal vectors to  $\mathcal{S}_{\epsilon\delta}$  by  $\mathbf{t}_{\epsilon\delta}^\alpha(\mathbf{x})$ ,  $\alpha = 1, \dots, d-1$ , and  $\mathbf{n}_{\epsilon\delta}(\mathbf{x})$ , respectively,

$$\mathbf{t}_{\epsilon\delta}^\alpha(\mathbf{x}) = \mathbf{t}^\alpha(\mathbf{x}) + \epsilon \theta_\alpha(\mathbf{x}) \mathbf{e}_d + O(\epsilon^2), \quad (3.23)$$

$$\mathbf{n}_{\epsilon\delta}(\mathbf{x}) = \mathbf{n}(\mathbf{x}) - \epsilon \sum_{\alpha=1}^{d-1} \theta_\alpha(\mathbf{x}) \mathbf{e}_\alpha + O(\epsilon^2), \quad (3.24)$$

with  $\theta_\alpha(\mathbf{x}) = \mathbf{e}_\alpha \cdot \nabla \delta(\mathbf{x})$ . Hence, by (3.16),

$$\left. \begin{aligned} \mathbf{t}^\alpha \cdot \boldsymbol{\tau}(\mathbf{v}) \cdot \mathbf{n} + \epsilon \left( \theta_\alpha \mathbf{n} \cdot \boldsymbol{\tau}(\mathbf{v}) \cdot \mathbf{n} - \mathbf{t}^\alpha \cdot \boldsymbol{\tau}(\mathbf{v}) \cdot \sum_{\beta=1}^{d-1} \theta_\beta \mathbf{t}^\beta + \mathbf{t}^\alpha \cdot \boldsymbol{\tau}(\delta \mathbf{e}_d \cdot \nabla \mathbf{v}) \cdot \mathbf{n} \right) = 0 \\ \mathbf{v} \cdot \nabla p + \epsilon \delta \mathbf{e}_d \cdot \nabla (\mathbf{v} \cdot \nabla p) = 0 \end{aligned} \right\}, \quad (3.25)$$

specifies the quasi implicit boundary conditions on  $\mathcal{S}$ . One infers that the above boundary conditions are equivalent to (3.2c) for  $\delta(\mathbf{x})$  according to (3.21) or (3.22): at the free-boundary  $p(\mathbf{x})$  vanishes and, as a consequence,  $\delta(\mathbf{x})$  and  $\theta(\mathbf{x})$  vanish. Hence, the parenthesized terms in (3.25) disappear and (3.25) reduces to (3.2c).

If (3.25) is imposed at  $\mathcal{S}$  and, subsequently, the boundary is modified to  $\mathcal{S}_{\epsilon\delta}$  and (3.2c) is imposed, then the disturbance thus introduced is  $O(\epsilon^2)$ . If, instead, a suitable approximation to (3.25) is imposed, then one can regard the approximation as a perturbation of (3.25). Assuming that the associated boundary value problem is well-posed, the change in the solution is bounded by the change in the boundary conditions. Hence, if an  $O(\epsilon)$  approximation instead of (3.25) is imposed at  $\mathcal{S}$ , then the induced disturbance is bounded by the difference between the approximation and (3.25). Therefore, anticipating that a term in (3.25) is relatively small, this term can be neglected. In particular, one should note that if  $\mathbf{v}(\mathbf{x})$  is smooth in  $x_d$ ,  $\nabla p(\mathbf{x})$  is smooth in  $\mathbf{x}$  and, correspondingly,  $\delta(\mathbf{x})$  is smooth in  $\mathbf{x}$  at  $\mathcal{S}$ , then the terms between parentheses can be omitted entirely. For example, considering perturbations of a uniform flow,

$$\mathbf{v}(\mathbf{x}) = \mathbf{v}^{(0)} + \epsilon \mathbf{v}^{(1)}(\mathbf{x}), \quad (3.26)$$

$$p(\mathbf{x}) = -\text{Fr}^{-2} x_d + \epsilon p^{(1)}(\mathbf{x}), \quad (3.27)$$

for constant  $\mathbf{v}^{(0)}$ , the terms between parentheses in (3.25) are of  $O(\epsilon)$  and can properly be disregarded.

Alternatively, in an iterative method, the relatively small contributions to the quasi-implicit boundary condition can be included by means of a defect correction process (see, e.g., [2]). In any case, convergence of the descent method is obviously ensured if the argument of the cost functional is reduced. Ignoring terms  $O(\epsilon^2)$ , this translates into the following requirement for the induced disturbance and the approximate descent step:

$$|p_{\tilde{\epsilon}\delta}(\mathbf{x} + \tilde{\epsilon}\delta(\mathbf{x}) \mathbf{e}_d)| = |p(\mathbf{x}) + \tilde{\epsilon}\delta(\mathbf{x}) \mathbf{e}_d \cdot \nabla p(\mathbf{x}) + p'_{\tilde{\epsilon}\delta}(\mathbf{x})| < |p(\mathbf{x})|, \quad \mathbf{x} \in \mathcal{S}, \quad (3.28)$$

or, equivalently,

$$\left| 1 + \frac{\tilde{\epsilon}\delta(\mathbf{x}) \mathbf{e}_d \cdot \nabla p(\mathbf{x}) p'_{\tilde{\epsilon}\delta}(\mathbf{x})}{p(\mathbf{x})} \right| \leq \zeta < 1, \quad \mathbf{x} \in \mathcal{S} \quad (3.29)$$

for some positive constant  $\zeta$ . In conclusion, if (3.29) is satisfied for a certain choice of the approximate quasi-implicit boundary condition and the approximate descent step, then the associated descent method converges with contraction number  $\zeta$ .

#### 4. DISCRETIZATION

We consider the discretization of the incompressible Navier-Stokes equations, implemented in `parnax`. The discretization is essentially analogous to the one described in [16]. The discrete equations derive from a finite volume discretization of the reduced Reynolds averaged Navier-Stokes equations and the corresponding boundary conditions in 2 space-dimensions. A mixed Cartesian/contravariant formulation in curvilinear coordinates is adopted, to allow use of a boundary fitted, structured grid without the occurrence of Christoffel symbols.

The equations are reduced by omitting the diffusive contribution to the momentum equations in one coordinate direction. This renders the reduced equations partially parabolic, which facilitates the solution of the corresponding system of discrete equations.

Following [7, 11], to arrive at a consistent and stable discretization, symmetric upwind/downwind biased differencing of the velocity gradients in the continuity equation (2.1a) and the pressure gradient in the momentum equation (2.1b) is used. In [7] it is shown that if first order finite differences are used, the resulting discretization is unconditionally stable and convergent. This approach permits the use of collocated grids, instead of staggered grids (see, e.g., [3, 13]).

##### 4.1 Scalar decomposition and reduction

Let  $T : \boldsymbol{\xi} \mapsto \mathbf{x}(\boldsymbol{\xi})$ ,  $\boldsymbol{\xi} \in \Omega \subset \mathbb{R}^d$ ,  $\mathbf{x} \in \mathcal{G} \subset \mathbb{R}^d$  denote an admissible transformation from a computational domain to a physical domain. A transformation is admissible if it has the properties:

(i)  $T$  is bijective.

(ii)  $T$  is differentiable and the Jacobian,

$$\sqrt{g} = \left| \frac{\partial \mathbf{x}}{\partial \boldsymbol{\xi}} \right| = \begin{vmatrix} \frac{\partial x^1}{\partial \xi^1} & \frac{\partial x^2}{\partial \xi^1} & \cdots & \frac{\partial x^d}{\partial \xi^1} \\ \vdots & \vdots & & \vdots \\ \frac{\partial x^1}{\partial \xi^2} & \frac{\partial x^2}{\partial \xi^2} & \cdots & \frac{\partial x^d}{\partial \xi^2} \end{vmatrix}, \quad \boldsymbol{\xi} \in \Omega, \quad (4.1)$$

is bounded and non-zero.

Next, covariant and contravariant base vectors are defined by

$$\mathbf{a}_{(\alpha)} = \partial \mathbf{x} / \partial \xi^\alpha, \quad \mathbf{a}^{(\alpha)} = \nabla \xi^\alpha. \quad (4.2)$$

Covariant and contravariant tensor components will be indicated by Greek sub- and superscripts, respectively. For example,  $v^\alpha = \mathbf{v} \cdot \mathbf{a}^{(\alpha)}$  and  $v_\alpha = \mathbf{v} \cdot \mathbf{a}_{(\alpha)}$  and, conversely,  $\mathbf{v} = v^\alpha \mathbf{a}_{(\alpha)} = v_\alpha \mathbf{a}^{(\alpha)}$ . Cartesian tensor components will be indicated by underlined Greek indices, to distinguish from covariant and contravariant components.

Introducing the momentum-flux tensor

$$\mathbf{W}(\mathbf{v}, \varphi) = \mathbf{v} \mathbf{v} + \mathbf{I} \varphi - \boldsymbol{\tau}(\mathbf{v}), \quad (4.3a)$$

with  $\mathbf{I}$  the unit tensor, equation (2.1b) in steady form can be rewritten as

$$\operatorname{div} \mathbf{W}(\mathbf{v}, \varphi) = 0. \quad (4.3b)$$

A scalar decomposition in contravariant components of the momentum-flux tensor and the equation vector and covariant differentiation then yields for (4.3b)

$$W_{,\beta}^{\alpha\beta} = \frac{\partial W^{\alpha\beta}}{\partial \xi^\beta} + \left\{ \begin{matrix} \beta \\ \gamma \beta \end{matrix} \right\} W^{\alpha\gamma} + \left\{ \begin{matrix} \alpha \\ \gamma \beta \end{matrix} \right\} W^{\gamma\beta} = \frac{1}{\sqrt{g}} \frac{\partial \sqrt{g} W^{\alpha\beta}}{\partial \xi^\beta} + \left\{ \begin{matrix} \alpha \\ \gamma \beta \end{matrix} \right\} W^{\gamma\beta} = 0. \quad (4.4)$$

where

$$\left\{ \begin{matrix} \alpha \\ \gamma \beta \end{matrix} \right\} = \frac{\partial \mathbf{a}_{(\gamma)}}{\partial \xi^\beta} \cdot \mathbf{a}^{(\alpha)} = \frac{\partial^2 x^\delta}{\partial \xi^\gamma \partial \xi^\beta} \frac{\partial \xi^\alpha}{\partial x^\delta} \quad (4.5)$$

is the so-called Christoffel symbol of the second kind, see, e.g., [1]. From (4.5) it is apparent that the Christoffel symbol comprises second order derivatives of the coordinate transformation. Consequently, a discrete approximation of the Christoffel symbol will be inaccurate if the transformation is unsmooth.

The occurrence of Christoffel symbols can be conveniently avoided by decomposing the momentum-flux tensor in mixed Cartesian/contravariant components. For the scalar decomposition of (4.3b) one then obtains

$$W_{,\beta}^{\alpha\beta} = \frac{1}{\sqrt{g}} \frac{\partial \sqrt{g} W^{\alpha\beta}}{\partial \xi^\beta} = 0. \quad (4.6)$$

This is the approach adopted here. Expanding  $\mathbf{W}$  results in

$$\frac{1}{\sqrt{g}} \frac{\partial}{\partial \xi^\beta} \sqrt{g} \left( v^\alpha v^\beta + a^{(\beta)\underline{\alpha}} \varphi - \operatorname{Re}^{-1} \left[ g^{\beta\gamma} \frac{\partial v^\alpha}{\partial \xi^\gamma} + a^{(\gamma)\underline{\alpha}} a_{\underline{\delta}}^{(\beta)} \frac{\partial v^{\underline{\delta}}}{\partial \xi^\gamma} \right] \right) = 0, \quad (4.7)$$

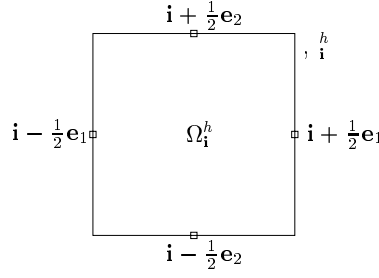


**Figure 2:** Cell  $\Omega_i^h$  with boundary  $\Gamma_i^h$  and boundary midpoints.

with  $a^{(\beta)\underline{\alpha}} = \mathbf{a}^{(\beta)} \cdot \mathbf{e}^{(\underline{\alpha})}$  the Cartesian  $\underline{\alpha}$ -component of the contravariant base vector and the contravariant metric tensor  $g^{\beta\gamma} = \mathbf{a}^{(\beta)} \cdot \mathbf{a}^{(\gamma)}$ . Here we have used the incompressibility constraint to reduce the viscous term. Notice that the reduction (2.2) is not allowed, because the Reynolds number is not spatially invariant due to the use of a turbulence model.

In `parmax`, a discretization of reduced incompressible Navier-Stokes is implemented. The reduction consists of discarding the viscous contribution to (4.7) in one general coordinate direction. In particular, if the equations are reduced in the  $\xi^1$ -direction, all derivatives in the  $\xi^1$ -direction that occur in the viscous term are omitted. This implies that the term in brackets is ignored if either  $\beta$  or  $\gamma$  assumes the value 1. The corresponding reduced momentum-flux tensor will be denoted by  $\underline{\mathbf{W}}$ .

For the incompressibility condition (2.1a), a scalar decomposition of the velocity vector in contravariant components is used:

$$v_{,\alpha}^{\alpha} = \frac{1}{\sqrt{g}} \frac{\partial \sqrt{g} v^{\alpha}}{\partial \xi^{\alpha}} = 0. \quad (4.8)$$

#### 4.2 Discretization

We discuss the finite volume discretization employed in `parmax`. Let  $\mathcal{V} \subset \mathbb{R}^2$  denote the domain of definition of (2.1), and let  $\Omega \subset \mathbb{R}^2$  denote a reference domain, i.e.,  $T: \Omega \mapsto \mathcal{V}$ . We suppose that the reference domain is composed of cells  $\Omega_i = \{\boldsymbol{\xi} \in \mathbb{R}^2 \mid i^{\alpha} - \frac{1}{2} < \xi^{\alpha} < i^{\alpha} + \frac{1}{2}\}$ , with the multi-index  $\mathbf{i} = (i^1, i^2) \in \mathbb{Z}^2$ ; see Figure 2. The corresponding cells in  $\mathcal{V}$  are denoted by  $\mathcal{V}_i^h = T(\Omega_i^h)$ .

We integrate (2.1a) over a cell  $\mathcal{V}_i^h$ . Then, we substitute (4.8) and apply the divergence theorem to the result. Thus, we obtain,

$$\int_{\mathcal{V}_i^h} \operatorname{div} \mathbf{v} \, d\mathcal{V} = \int_{\Omega_i^h} \frac{\partial \sqrt{g} v^{\alpha}}{\partial \xi^{\alpha}} \, d\Omega = \oint_{\Gamma_i^h} \sqrt{g} v^{\alpha} n_{\alpha} \, d, = 0, \quad (4.9)$$

where  $\Gamma_i^h$  denotes the boundary of  $\Omega_i^h$  and  $n_{\alpha}$  its outward unit normal vector. At the expense of a discretization error, the integral over the cell-boundary is on each side approximated by the midpoint rule, and we obtain the difference equation

$$\sum_{\alpha=1}^2 (\sqrt{g} v^{\alpha}) (\mathbf{x}(\boldsymbol{\xi})) \Big|_{\mathbf{i}-\frac{1}{2}\mathbf{e}_{\alpha}}^{\mathbf{i}+\frac{1}{2}\mathbf{e}_{\alpha}} = 0. \quad (4.10)$$

Similarly, we obtain for (4.3b), with  $\mathbf{W}$  replaced by  $\underline{\mathbf{W}}$ ,

$$\int_{\mathcal{V}_i^h} \operatorname{div} \underline{\mathbf{W}} \, d\mathcal{V} = \int_{\Omega_i^h} \mathbf{e}_{(\underline{\alpha})} \frac{\partial \sqrt{g} \underline{W}^{\alpha\beta}}{\partial \xi^{\beta}} \, d\Omega = \mathbf{e}_{(\underline{\alpha})} \oint_{\Gamma_i^h} \sqrt{g} \underline{W}^{\alpha\beta} n_{\beta} \, d, = \mathbf{0}. \quad (4.11)$$

Upon projecting (4.11) onto  $\mathbf{e}^{(\underline{\alpha})}$  and approximating the boundary-integrals, we obtain the system of

difference equations: for  $\alpha = 1, 2$ ,

$$\sum_{\beta=1}^2 \left( \sqrt{g} W^{\alpha\beta} \right) (\mathbf{x}(\boldsymbol{\xi})) \Big|_{\mathbf{i}-\frac{1}{2}\mathbf{e}_\alpha}^{\mathbf{i}+\frac{1}{2}\mathbf{e}_\alpha} = 0. \quad (4.12)$$

A collocated, centered grid arrangement is employed, i.e., the boundary midpoint values of  $\mathbf{v}(\mathbf{x}(\boldsymbol{\xi}))$  and  $\varphi(\mathbf{x}(\boldsymbol{\xi}))$  in difference equations (4.10) and (4.12) are approximated by an interpolation from values at the cell-centers. Below, we give some details of the interpolations.

Let grid-functions  $\mathbf{v}_h : \mathbb{Z}^2 \mapsto \mathbb{R}^2$  and  $\varphi_h : \mathbb{Z}^2 \mapsto \mathbb{R}$  approximate  $\mathbf{v}(\mathbf{x})$  and  $\varphi(\mathbf{x})$  at cell-centers. The velocity vector in equation (4.10) is approximated by interpolation from the values  $\mathbf{v}_h$  as

$$\mathbf{v}_{\mathbf{i}+\frac{1}{2}\mathbf{e}_1} = \frac{3}{2}\mathbf{v}_h(\mathbf{i}) - \frac{1}{2}\mathbf{v}_h(\mathbf{i} - \mathbf{e}_1), \quad (4.13a)$$

$$\mathbf{v}_{\mathbf{i}+\frac{1}{2}\mathbf{e}_2} = \frac{3}{8}\mathbf{v}_h(\mathbf{i} + \mathbf{e}_2) + \frac{3}{4}\mathbf{v}_h(\mathbf{i}) - \frac{1}{8}\mathbf{v}_h(\mathbf{i} - \mathbf{e}_2). \quad (4.13b)$$

The pressure at boundary midpoints in (4.12) is approximated by interpolation from  $\varphi_h$ :

$$\varphi_{\mathbf{i}+\frac{1}{2}\mathbf{e}_1} = \frac{3}{2}\varphi_h(\mathbf{i}) - \frac{1}{2}\varphi_h(\mathbf{i} + \mathbf{e}_1), \quad (4.14a)$$

$$\varphi_{\mathbf{i}+\frac{1}{2}\mathbf{e}_2} = \frac{3}{8}\varphi_h(\mathbf{i}) + \frac{3}{4}\varphi_h(\mathbf{i} + \mathbf{e}_2) - \frac{1}{8}\varphi_h(\mathbf{i} + 2\mathbf{e}_2). \quad (4.14b)$$

Note that the interpolation stencils used in (4.13) and (4.14) are symmetric. This symmetry is essential for maintaining certain important properties of the continuum operator, see Section 5.1. A second velocity vector is interpolated at the boundary midpoints:

$$\bar{\mathbf{v}}_{\mathbf{i}+\frac{1}{2}\mathbf{e}_1} = \begin{cases} \mathbf{v}_{\mathbf{i}+\frac{1}{2}\mathbf{e}_1}, & v_{\mathbf{i}+\frac{1}{2}\mathbf{e}_1}^1 \geq 0, \\ \mathbf{0}, & \text{otherwise,} \end{cases} \quad (4.15a)$$

$$\bar{\mathbf{v}}_{\mathbf{i}+\frac{1}{2}\mathbf{e}_2} = \begin{cases} \mathbf{v}_{\mathbf{i}+\frac{1}{2}\mathbf{e}_1}, & v_{\mathbf{i}+\frac{1}{2}\mathbf{e}_2}^2 \geq 0, \\ \underline{\mathbf{v}}_{\mathbf{i}+\frac{1}{2}\mathbf{e}_2}, & \text{otherwise,} \end{cases} \quad (4.15b)$$

where,

$$\underline{\mathbf{v}}_{\mathbf{i}+\frac{1}{2}\mathbf{e}_2} = \frac{3}{8}\mathbf{v}_h(\mathbf{i}) + \frac{3}{4}\mathbf{v}_h(\mathbf{i} + \mathbf{e}_2) - \frac{1}{8}\mathbf{v}_h(\mathbf{i} + 2\mathbf{e}_2). \quad (4.15c)$$

The Cartesian velocity components in the convective contribution to (4.12) are then obtained from (4.15), whereas the contravariant velocity components are obtained from (4.13).

Due to the reduction of the viscous term, only the velocity derivative  $(\partial\mathbf{v}/\partial\xi^2)_{\mathbf{i}+\frac{1}{2}\mathbf{e}_2}$  is required for computing the viscous-flux contribution. This derivative is approximated by a central difference:

$$\left( \frac{\partial\mathbf{v}}{\partial\xi^2} \right)_{\mathbf{i}+\frac{1}{2}\mathbf{e}_2} = \mathbf{v}_h(\mathbf{i} + \mathbf{e}_2) - \mathbf{v}_h(\mathbf{i}). \quad (4.16)$$

To close the discussion of the discretization of (2.1), the covariant and contravariant vectors and the associated metric quantities have to be specified. In cell-centers these follow immediately from the assumption that the transformation,  $T$ , is a piecewise bi-linear interpolation from  $\Omega_i^h$  to  $\mathcal{V}_i^h$ . The value at boundary midpoints is obtained as the average of the value at the centers of adjacent cells.

#### 4.3 Discretization of boundary conditions

Generally, either Neumann or Dirichlet conditions are imposed on all boundaries except the quasi free-surface. The discretization of these boundary conditions is straightforward and will not be discussed.

The discretization of the quasi free-surface condition, however, requires elaboration. Scalar decomposition of the steady quasi free-surface condition, (2.9), yields

$$\mathbf{v} \cdot \nabla (\varphi - \text{Fr}^{-2} x_d) = v^\alpha \mathbf{a}_\alpha^{(\beta)} \frac{\partial \varphi}{\partial \xi^\beta} - \text{Fr}^{-2} v^2 = 0. \quad (4.17)$$

The quasi free-surface condition is a hyperbolic type convection equation for pressure disturbances. Hence, in the dominant flow direction we choose an upwind biased discretization of the pressure derivative in (4.17). Specifically, associating the free surface with cell-boundaries and the  $\xi^1$ -direction with the dominant flow direction,

$$\left( \frac{\partial \varphi}{\partial \xi^1} \right)_{\mathbf{i} + \frac{1}{2} \mathbf{e}_2} = \frac{3}{2} \varphi_{\mathbf{i} + \frac{1}{2} \mathbf{e}_2} - 2 \varphi_{\mathbf{i} + \frac{1}{2} \mathbf{e}_2 - \mathbf{e}_1} + \frac{1}{2} \varphi_{\mathbf{i} + \frac{1}{2} \mathbf{e}_2 - 2 \mathbf{e}_1}, \quad \mathbf{x}(\mathbf{i} + \frac{1}{2} \mathbf{e}_2) \in \mathcal{S}, \quad (4.18)$$

with the boundary midpoint values  $\varphi_{\mathbf{i} + \frac{1}{2} \mathbf{e}_2}$  according to (4.14). The  $\xi^2$ -derivative of the pressure is approximated as

$$\left( \frac{\partial \varphi}{\partial \xi^2} \right)_{\mathbf{i} + \frac{1}{2} \mathbf{e}_2} = \varphi_h(\mathbf{i} + \mathbf{e}_2) - \varphi_h(\mathbf{i}), \quad \mathbf{x}(\mathbf{i} + \frac{1}{2} \mathbf{e}_2) \in \mathcal{S}. \quad (4.19)$$

One may note that (4.19) involves values of  $\varphi_h(\mathbf{i})$  located beyond the boundary  $\mathcal{S}$ . Such virtual nodes merely serve to convenience notation and implementation. The velocity components in discretized quasi free-surface condition are given by (4.13).

## 5. WAVE SOLUTIONS OF THE DISCRETE EQUATIONS

In [4] it was shown that the incompressible Navier-Stokes equations (2.1) subject to the quasi free-surface condition (2.9) allow infinitesimally stable wave solutions. These wave solutions exhibit a behavior that is dictated by the dispersion relation for the initial boundary value problem. For stationary waves in a channel of unit depth, this dispersion relation specifies a unique relation between the Froude number and the wavenumber:

$$k^{-1} \tanh(k) = \text{Fr}^2, \quad (5.1)$$

where  $k \equiv \lambda/2\pi$  is the wave-number and  $\lambda$  the wavelength.

In this section we derive a similar relation for the system of discrete equations introduced in Section 4. This relation will be referred to as a discrete dispersion relation. Furthermore, we derive the discrete dispersion relation for the case of infinite depth.

### 5.1 General infinitesimal solutions

We suppose that the Cartesian domain is partitioned in regular cells  $\{\mathbf{x} \in \mathbb{R}^2 \mid (i^\alpha - \frac{1}{2})h < x_\alpha < (i^\alpha + \frac{1}{2})h\}$ . The contravariant components in Sections 4.2 and 4.3 then identify with scaled Cartesian components (for example,  $v^\alpha = v^\alpha/h$ ) and the Jacobian of the transformation reduces to  $\sqrt{g} = h^2$ . Further, we assume the Reynolds number to be spatially invariant, thus ignoring effects of the turbulence model.

We consider the semi-discrete incompressible reduced Navier-Stokes equations, i.e., (2.1) with the spatial operators replaced by their discrete counterparts as defined by (4.10), (4.12) and (4.13) through (4.16). Let grid-functions  $\mathbf{v}_h(\mathbf{i}, t)$  and  $\varphi_h(\mathbf{i}, t)$  approximate  $\mathbf{v}(\mathbf{x}, t)$  and  $\varphi(\mathbf{x}, t)$  in cell-centers, respectively. Then the resulting semi-discrete equations are written as

$$\left. \begin{aligned} \mathbf{N}_h(\mathbf{v}_h, \varphi_h) &= 0 \\ M_h(\mathbf{v}_h, \varphi_h) &= 0 \end{aligned} \right\} \quad \mathbf{i} \in \mathcal{V}_h, \quad t \geq 0, \quad (5.2)$$

where  $\mathcal{V}_h = \{\mathbf{i} \in \mathbb{Z}^2 \mid \mathbf{x}(\mathbf{i}) \in \mathcal{V}\}$ . Similarly,

$$K_h(\mathbf{v}_h, \varphi_h) = 0, \quad \mathbf{i} \in \mathcal{S}_h, \quad t \geq 0, \quad (5.3)$$

expresses the discrete quasi free-surface condition. Here  $\mathcal{S}_h$  is a set of nodes that we associate with the free boundary  $\mathcal{S}$ .

We consider solutions that are a perturbation of a uniform horizontal flow with velocity  ${}^0\mathbf{v}_h = ({}^0v^1, 0)$  for some constant  ${}^0v^1 \geq 0$  and with  ${}^0\varphi_h = 0$ . The perturbation is parameterized by  $\epsilon$ , such that

$$\begin{pmatrix} \mathbf{v}_h \\ \varphi_h \end{pmatrix}(\mathbf{i}, t; \epsilon) \sim \begin{pmatrix} {}^0\mathbf{v}_h \\ {}^0\varphi_h \end{pmatrix}(\mathbf{i}, t) + \epsilon \begin{pmatrix} {}^1\mathbf{v}_h \\ {}^1\varphi_h \end{pmatrix}(\mathbf{i}, t), \quad \text{for } \epsilon \rightarrow 0. \quad (5.4)$$

Inserting this asymptotic expansion in (5.2) and (5.3) and ignoring terms  $o(\epsilon)$ , we obtain:

$$\left. \begin{aligned} \underline{\mathbf{N}}_h({}^1\mathbf{v}_h, {}^1\varphi_h) &= 0 \\ M_h({}^1\mathbf{v}_h, {}^1\varphi_h) &= 0 \end{aligned} \right\} \quad \mathbf{i} \in \mathcal{V}_h, \quad t \geq 0, \quad (5.5a)$$

with  $\underline{\mathbf{N}}_h(\mathbf{v}_h, \varphi_h)$  the semi-discrete linear operator

$$\begin{aligned} \underline{\mathbf{N}}_h(\mathbf{v}_h, \varphi_h) \equiv & \sqrt{g} \frac{\partial \mathbf{v}_h}{\partial t} + \mathbf{e}_{(\alpha)} \sum_{\beta=1}^2 \left[ \sqrt{g} \left( v^\alpha {}^0v^\beta + a^{(\beta)\alpha} \varphi \right) \right] \Big|_{\mathbf{i} \Big|_{-\frac{1}{2}\mathbf{e}_\beta}}^{\mathbf{i} + \frac{1}{2}\mathbf{e}_\beta} \\ & - \mathbf{e}_{(\alpha)} \operatorname{Re}^{-1} \left[ \sqrt{g} \left( g^{22} \frac{\partial v^\alpha}{\partial \xi^2} + a^{(2)\alpha} a_{\underline{i}}^{(2)} \frac{\partial v^{\underline{d}}}{\partial \xi^2} \right) \right] \Big|_{\mathbf{i} \Big|_{-\frac{1}{2}\mathbf{e}_2}}^{\mathbf{i} + \frac{1}{2}\mathbf{e}_2}, \end{aligned} \quad (5.5b)$$

and corresponding quasi free-surface conditions

$$\underline{\mathbf{K}}_h({}^1\mathbf{v}_h, {}^1\varphi_h) = 0, \quad \mathbf{i} \in \mathcal{S}_h, \quad t \geq 0, \quad (5.6)$$

where,

$$\underline{\mathbf{K}}_h(\mathbf{v}_h, \varphi_h) \equiv \frac{\partial \varphi_h}{\partial t} + {}^0v^\alpha \left( \frac{\partial \varphi}{\partial \xi^\alpha} \right)_{\mathbf{i} + \frac{1}{2}\mathbf{e}_2} - \operatorname{Fr}^{-2} v_{\mathbf{i} + \frac{1}{2}\mathbf{e}_2}^2. \quad (5.7)$$

The non-linearity of the momentum equations (5.2) and the kinematic condition (5.3) is of  $o(\epsilon)$  and vanishes in the first term of the expansion.

Next, we derive general solutions for the first-order equations (5.5). For convenience, we introduce the notation  $\mathbf{q}_h = ({}^1v_h^1, {}^1v_h^2, {}^1\varphi_h)$ . We suppose that  $\mathbf{q}_h$  can be written as:

$$\mathbf{q}_h(\mathbf{i}, t) = \int_{\Theta} \int_{\mathbb{C}} \hat{\mathbf{q}}(\boldsymbol{\theta}, \tau) e^{\tau t + \boldsymbol{\theta} \cdot \mathbf{x}(\mathbf{i})} d\tau d\boldsymbol{\theta}. \quad (5.8)$$

The integration is taken over all  $\tau \in \mathbb{C}$  and all  $\boldsymbol{\theta} \in \Theta = \{\boldsymbol{\theta} \in \mathbb{C}^2 \mid -\pi/h < \Im(\theta_\alpha) \leq \pi/h\}$ , a strip in  $\mathbb{C}^2$ . The function  $\hat{\mathbf{q}}(\boldsymbol{\theta}, \tau)$  is to be understood in a generalized sense; see, e.g., [20]. In particular,  $\hat{\mathbf{q}}(\boldsymbol{\theta}, \tau)$  is allowed to vanish almost everywhere in  $\Theta \times \mathbb{C}$ .

Inserting (5.8) into (5.5) and changing the order of operations:

$$\mathbf{P}_h(\mathbf{q}_h) \equiv \begin{pmatrix} \underline{\mathbf{N}}_h \\ M_h \end{pmatrix}(\mathbf{q}_h) = \int_{\Theta} \int_{\mathbb{C}} \widehat{\mathbf{P}}_h(\boldsymbol{\theta}, \tau) \cdot \hat{\mathbf{q}}(\boldsymbol{\theta}, \tau) e^{\tau t + \boldsymbol{\theta} \cdot \mathbf{x}(\mathbf{i})} d\tau d\boldsymbol{\theta}, \quad (5.9)$$

with the symbol  $\widehat{\mathbf{P}}_h$  defined by

$$\widehat{\mathbf{P}}_h(\boldsymbol{\theta}, \tau) = h^2 \begin{pmatrix} \widehat{H}_h(\boldsymbol{\theta}, \tau) + \widehat{\sigma}_h(\boldsymbol{\theta}) & 0 & \widehat{\partial}_{\mathbf{p}_h^1}(\theta_1) \\ 0 & \widehat{H}_h(\boldsymbol{\theta}, \tau) + 2\widehat{\sigma}_h(\boldsymbol{\theta}) & \widehat{\partial}_{\mathbf{p}_h^2}(\theta_2) \\ \widehat{\partial}_{\mathbf{d}_h^1}(\theta_1) & \widehat{\partial}_{\mathbf{d}_h^2}(\theta_2) & 0 \end{pmatrix}, \quad (5.10a)$$

where

$$\widehat{H}_h(\boldsymbol{\theta}, \tau) = \tau + {}^0v^1 \widehat{\partial}_{c_h^1}(\theta_1), \quad (5.10b)$$

$$\widehat{\sigma}_h(\boldsymbol{\theta}) = \text{Re}^{-1} \widehat{\Delta}_h^2(\theta_2). \quad (5.10c)$$

Here,  $\widehat{\partial}_{c_h^\alpha}(\theta_\alpha)$  and  $\widehat{\partial}_{p_h^\alpha}(\theta_\alpha)$  denote the symbols of the discrete approximations to the  $\xi^\alpha$ -derivatives of the velocity and the pressure in  $\mathbf{N}_h$ , and  $\widehat{\partial}_{d_h^\alpha}(\theta_\alpha)$  is the symbol of the approximation to the velocity derivatives in  $M_h$ . In formulas,  $\widehat{\partial}_{c_h^\alpha}(\theta_\alpha) = \widehat{\partial}_{d_h^\alpha}(\theta_\alpha) = -\widehat{\partial}_{p_h^\alpha}(-\theta_\alpha)$ , with

$$\widehat{\partial}_{p_h^1}(\theta_1) = h^{-1} \left( -\frac{3}{2} + 2e^{h\theta_1} - \frac{1}{2}e^{2h\theta_1} \right), \quad (5.11)$$

$$\widehat{\partial}_{p_h^2}(\theta_2) = h^{-1} \left( -\frac{3}{8}e^{-h\theta_2} - \frac{3}{8} + \frac{7}{8}e^{h\theta_2} - \frac{1}{8}e^{2h\theta_2} \right), \quad (5.12)$$

and

$$\widehat{\Delta}_h^2(\theta_2) = h^{-2} (e^{h\theta_2} - 2 + e^{-h\theta_2}). \quad (5.13)$$

The values of  $\boldsymbol{\theta}$  and  $\tau$  that satisfy the characteristic equation

$$\det(\widehat{\mathbf{P}}_h(\boldsymbol{\theta}, \tau)) = - \left( \widehat{\partial}_{p_h^1} \widehat{\partial}_{d_h^1} + \widehat{\partial}_{p_h^2} \widehat{\partial}_{d_h^2} \right) \left( \widehat{H}_h + \widehat{\sigma}_h \right) - \widehat{\sigma}_h \widehat{\partial}_{p_h^1} \widehat{\partial}_{d_h^1} = 0, \quad (5.14)$$

correspond to nontrivial homogeneous solutions of  $\mathbf{P}_h(\mathbf{q}_h)$  and, hence, to solutions of (5.5).

The characteristic equation (5.14) is similar to the characteristic equation corresponding to the incompressible Navier-Stokes equations (2.1) [4]:

$$\det(\widehat{\mathbf{P}}(\boldsymbol{\theta}, \tau)) = -(\boldsymbol{\theta} \cdot \boldsymbol{\theta})(\tau + {}^0\mathbf{v} \cdot \boldsymbol{\theta} - \text{Re}^{-1} \boldsymbol{\theta} \cdot \boldsymbol{\theta}) = 0. \quad (5.15)$$

Comparing both characteristic equations in the high Reynolds-number limit, it becomes apparent that the first term between parentheses in (5.14) is an approximation to the symbol  $\boldsymbol{\theta} \cdot \boldsymbol{\theta}$  in (5.15). More precisely,  $\widehat{\partial}_{p_h^\alpha} \widehat{\partial}_{d_h^\alpha}$  is an approximation to  $\theta_\alpha^2$ . The symmetry condition,

$$\widehat{\partial}_{d_h^\alpha}(-\theta_\alpha) = -\widehat{\partial}_{p_h^\alpha}(\theta_\alpha), \quad (5.16)$$

ensures that certain important characteristic features of the symbol  $\theta_\alpha^2$  are maintained:

- (i) Let  $\zeta \in \mathbb{C}$ , then  $(-\zeta)^2 = \zeta^2$  and similarly  $\widehat{\partial}_{p_h^\alpha}(-\zeta) \widehat{\partial}_{d_h^\alpha}(-\zeta) = \widehat{\partial}_{p_h^\alpha}(\zeta) \widehat{\partial}_{d_h^\alpha}(\zeta)$ .
- (ii) Let  $\zeta \in \mathbb{R}$ , then  $\Im((i\zeta)^2) = 0$  and similarly  $\Im(\widehat{\partial}_{p_h^\alpha}(i\zeta) \widehat{\partial}_{d_h^\alpha}(i\zeta)) = 0$ .

Property (i) is easily proved. Property (ii) follows from the general form of the discrete symbols: Let  $n, q \in \mathbb{N}$  and  $c_l \in \mathbb{R}$  for  $l = 1, 2, \dots, n$ . Then,

$$\widehat{\partial}_{p_h^\alpha}(i\zeta) \widehat{\partial}_{d_h^\alpha}(i\zeta) = - \sum_{l=1}^n c_l e^{i(l-q)\zeta h} \sum_{k=1}^n c_k e^{i(q-k)\zeta h} = - \sum_{l=1}^n c_l^2 - \sum_{l=1}^n \sum_{k=1}^{l-1} 2c_l c_k \cos((l-k)\zeta h), \quad (5.17)$$

which clearly has vanishing imaginary part. The relevance of these properties will become clear in Section 5.2.

Further in this section, we will only consider the high Reynolds number case. Because of the linearity of  $\mathbf{P}_h$ , any homogeneous solution can be expressed as a linear combination of the homogeneous solutions corresponding to the roots of the characteristic equation. Let  $\{\hat{\mathbf{q}}_1(\boldsymbol{\theta}, \tau), \dots, \hat{\mathbf{q}}_n(\boldsymbol{\theta}, \tau)\}$ ,  $n =$

$\dim(\ker(\widehat{\mathbf{P}}_h(\boldsymbol{\theta}, \tau)))$ , denote a basis of the kernel of the symbol, e.g., if  $\widehat{\partial}_{\mathbf{p}_h^1} \widehat{\partial}_{\mathbf{d}_h^1} + \widehat{\partial}_{\mathbf{p}_h^2} \widehat{\partial}_{\mathbf{d}_h^2} = 0$  and  $\widehat{H}_h(\boldsymbol{\theta}, \tau) \neq 0$ , then  $n = 1$  and

$$\hat{\mathbf{q}}_1(\boldsymbol{\theta}, \tau) = \begin{pmatrix} \widehat{\partial}_{\mathbf{p}_h^1}(\theta_1) \\ \widehat{\partial}_{\mathbf{p}_h^2}(\theta_2) \\ -\widehat{H}_h(\boldsymbol{\theta}, \tau) \end{pmatrix}. \quad (5.18)$$

A general homogeneous solution to (5.5) can then be expressed as

$$\mathbf{q}_h(\mathbf{i}, t) = \int_{\Theta} \int_{\mathbb{C}} \sum_{j=1}^n w_j(\boldsymbol{\theta}, \tau) \hat{\mathbf{q}}_j(\boldsymbol{\theta}, \tau) e^{\tau t + \boldsymbol{\theta} \cdot \mathbf{x}(\mathbf{i})} d\tau d\boldsymbol{\theta}, \quad (5.19)$$

for certain weight-functions  $w_j(\boldsymbol{\theta}, \tau)$ . In order for the semi-discrete initial boundary value problem to be well-posed, the weight-functions must be uniquely determined by the boundary and initial conditions, in such a manner that  $\mathbf{q}_h(\mathbf{i}, t)$  remains bounded (in some suitable norm) on the domain of definition.

### 5.2 Finite depth wave solutions

We consider the semi-discrete equations (5.2) on a domain  $\mathcal{V} = \mathbb{R} \times [0, 1]$  with , for  $t \geq 0$ , subject to the quasi free-surface condition (5.6) and the impermeability condition at the bottom:

$$v_{\mathbf{i} + \frac{1}{2}\mathbf{e}_2}^2 = 0, \quad x^2(\mathbf{i} + \frac{1}{2}\mathbf{e}_2) = -1. \quad (5.20)$$

Additional boundary conditions are required to make the semi-discrete initial boundary value problem well-posed. However, we will only consider a specific subclass of solutions, viz.,

$$\mathbf{q}_h(\mathbf{i}, t) = \int_{\mathcal{H}} \int_{\mathcal{T}} w_1(\boldsymbol{\theta}, \tau) \hat{\mathbf{q}}_1(\boldsymbol{\theta}, \tau) e^{\tau t + \boldsymbol{\theta} \cdot \mathbf{x}(\mathbf{i})} d\tau d\boldsymbol{\theta}, \quad (5.21)$$

with  $\mathcal{H} = \{\boldsymbol{\theta} \in \Theta \mid \widehat{\partial}_{\mathbf{p}_h^1} \widehat{\partial}_{\mathbf{d}_h^1} + \widehat{\partial}_{\mathbf{p}_h^2} \widehat{\partial}_{\mathbf{d}_h^2} = 0\}$ ,  $\mathcal{T} = \{\tau \in \mathbb{C} \mid \widehat{H}_h(\boldsymbol{\theta}, \tau) \neq 0\}$  and, hence,  $\hat{\mathbf{q}}_1(\boldsymbol{\theta}, \tau)$  according to (5.18). From the previous section, we recall that  $\mathcal{H} \times \mathcal{T}$  corresponds to a subclass of solutions of the difference equation (5.5) for which the kernel of the symbol is spanned by  $\hat{\mathbf{q}}_1(\boldsymbol{\theta}, \tau)$  only. In the following, it will become evident that this subclass accommodates the gravity wave solutions. Hence, the subclass  $(\boldsymbol{\theta}, \tau) \in \mathcal{H} \times \mathcal{T}$  suffices for our purposes. For the above subclass it is sufficient to impose a single boundary condition on each boundary.

For convenience, we introduce  $\boldsymbol{\theta}^{\pm} \equiv (\theta_1, \pm\theta_2)$ . We divide  $\mathcal{H}$  in  $\mathcal{H}^+ = \{\boldsymbol{\theta} \in \mathcal{H} \mid \Re(\theta_2) \geq 0\}$  and  $\mathcal{H} \setminus \mathcal{H}^+$ . By symmetry property (i), we can rewrite (5.21) as:

$$\mathbf{q}_h(\mathbf{i}, t) = \int_{\mathcal{H}^+} \int_{\mathcal{T}} e^{\tau t} \left( w_1(\boldsymbol{\theta}^+, \tau) \hat{\mathbf{q}}_1(\boldsymbol{\theta}^+, \tau) e^{\boldsymbol{\theta}^+ \cdot \mathbf{x}(\mathbf{i})} + w_1(\boldsymbol{\theta}^-, \tau) \hat{\mathbf{q}}_1(\boldsymbol{\theta}^-, \tau) e^{\boldsymbol{\theta}^- \cdot \mathbf{x}(\mathbf{i})} \right) d\tau d\boldsymbol{\theta}. \quad (5.22)$$

Introducing equation (5.22) into the boundary condition (5.20) and requiring that the resulting integral vanishes, we obtain

$$w_1(\boldsymbol{\theta}^+, \tau) \widehat{\partial}_{\mathbf{p}_h^2}(\theta_2) \widehat{E}(\theta_2) + w_1(\boldsymbol{\theta}^-, \tau) \widehat{\partial}_{\mathbf{p}_h^2}(-\theta_2) \widehat{E}(-\theta_2) = 0, \quad (5.23)$$

with  $\widehat{E}(\theta_2)$  the symbol of the approximation to  $v^2$  at the boundary  $x_2 = -1$ , in particular, from equation (4.13),

$$\widehat{E}(\theta_2) = \frac{3}{8} e^{\theta_2(-1+\frac{1}{2}h)} + \frac{3}{4} e^{\theta_2(-1-\frac{1}{2}h)} - \frac{1}{8} e^{\theta_2(-1-\frac{3}{2}h)}. \quad (5.24)$$

This yields an expression for the weight function:

$$w_1(\boldsymbol{\theta}, \tau) = \gamma(\theta_1, \tau) \theta_2 \frac{\widehat{E}(-\theta_2)}{\widehat{\partial_{p_h}^2}(\theta_2)}, \quad (5.25)$$

for some suitable function  $\gamma(\theta_1, \tau)$ . Upon inserting the result, (5.25), into the quasi free-surface condition (5.6) and expanding  $\widehat{H}_h$ , we obtain the relation

$$\left(\tau + {}^0v^1 \widehat{\partial_{c_h}^1}(\theta_1)\right) \left(\tau + {}^0v^1 \widehat{\partial_{s_h}^1}(\theta_1)\right) = \text{Fr}^{-2} \frac{\widehat{E}(\theta_2) - \widehat{E}(-\theta_2)}{\frac{\widehat{E}(-\theta_2)}{\widehat{\partial_{p_h}^2}(\theta_2)} - \frac{\widehat{E}(\theta_2)}{\widehat{\partial_{p_h}^2}(-\theta_2)}}, \quad (5.26a)$$

with

$$\widehat{\partial_{s_h}^1}(\theta_1) = h^{-1} \left( \frac{3}{2} - 2e^{-h\theta_1} + \frac{1}{2}e^{-2h\theta_1} \right) \quad (5.26b)$$

the symbol of the discrete approximation to the  $\xi^1$ -pressure derivative in the quasi free-surface condition according to (4.18). Equation (5.26) can be regarded as a relation between temporal and spatial behavior of the solution. Such an expression for is usually called the dispersion relation for the initial boundary value problem.

A gravity wave solution of the continuous equations has strictly imaginary  $\theta_1$  and real  $\theta_2$ . Specifically, if the velocities are scaled such that  ${}^0v^1 = 1$ , then a stationary gravity wave solution ( $\tau = 0$ ) has  $\boldsymbol{\theta} = (ik, \pm k)$ , with the wavenumber,  $k$ , according to (5.1). Although the discrete difference equations (5.2) in principle permit such a solution due to symmetry property (ii), the upwind discretization of the quasi free-surface condition prohibits its existence. Hence, for stationary wave solutions of the discrete equations, generally  $\Re(\theta_1) \neq 0$  and  $\Im(\theta_2) \neq 0$ . Figure 3 displays the relative difference between the wavelength of a stationary wave solution of the continuous equations,  $\lambda$  according to (5.1), and the wavelength of a stationary wave solution of the discrete equations,  $\lambda_h = 2\pi/\Im(\theta_1)$  with  $\boldsymbol{\theta} \in \mathcal{H}^+$  a solution of (5.26) for  $\tau = 0$ , versus the Froude number, for various values of the mesh-width  $h$ . Figure 4 shows the associated wave attenuation per wavelength, defined by  $\nu_h = \exp(\Re(\theta_1) \lambda_h)$ .

### 5.3 Infinite depth wave solutions

We consider the semi-discrete equations (5.2) on the half space  $\mathcal{V} = \{\mathbf{x} \in \mathbb{R}^2 \mid -\infty < x_1 < \infty, -\infty < x_2 < 0\}$  for  $t \geq 0$ , subject to the quasi free-surface condition (5.6) and the condition

$$\lim_{x_2(\mathbf{i}) \rightarrow -\infty} v_h^2(\mathbf{i}, t) = 0, \quad t \geq 0. \quad (5.27)$$

Again, we only consider the specific subclass of solutions (5.21). Dividing the integration interval according to (5.22) and requiring (5.27) to hold, we find that

$$\lim_{x_2(\mathbf{i}) \rightarrow -\infty} w_1(\boldsymbol{\theta}^+, \tau) \widehat{\partial_{p_h}^2}(\theta_2) e^{\theta_2 x_2(\mathbf{i})} + w_1(\boldsymbol{\theta}^-, \tau) \widehat{\partial_{p_h}^2}(-\theta_2) e^{-\theta_2 x_2(\mathbf{i})} = 0. \quad (5.28)$$

Therefore,  $w_1(\boldsymbol{\theta}^-, \tau) = 0$ . Substituting the result into the quasi free-surface condition (5.6) and expanding  $\widehat{H}_h$ , we obtain the dispersion relation

$$\left(\tau + {}^0v^1 \widehat{\partial_{c_h}^1}(\theta_1)\right) \left(\tau + {}^0v^1 \widehat{\partial_{s_h}^1}(\theta_1)\right) = -\text{Fr}^{-2} \widehat{\partial_{p_h}^2}(\theta_2). \quad (5.29)$$

For  $\overline{\boldsymbol{\theta}} = 0$  and  ${}^0v^1 = 1$ , solutions of (5.30) should be compared to the corresponding dispersion relation of the continuous equations:

$$\boldsymbol{\theta} = (i \text{Fr}^{-2}, \text{Fr}^{-2}). \quad (5.30)$$

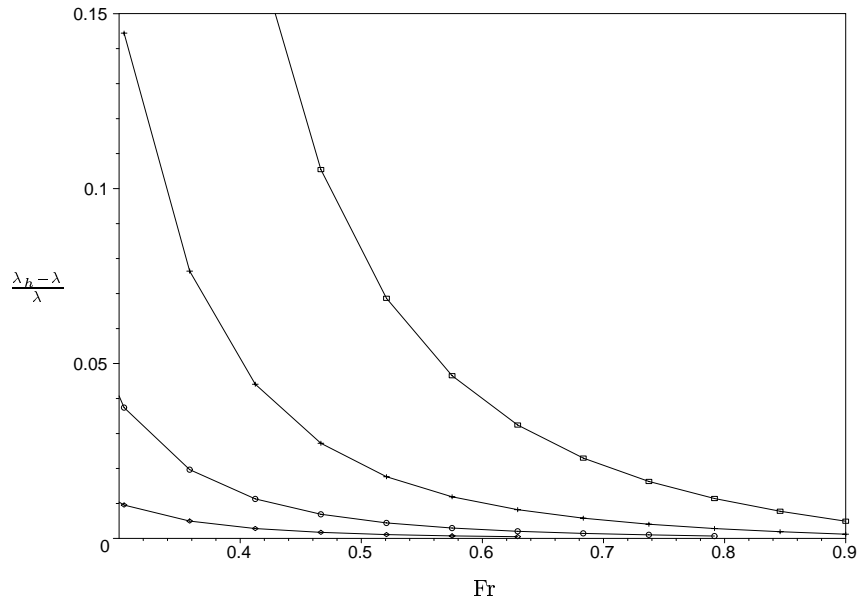


**Figure 3:** Relative difference between the wavelength of a stationary wave solution of the discrete equations and the wavelength of a stationary wave solution of the continuous equations versus the Froude number for mesh-width  $h = 2^{-l}$ ,  $l = 3$  ( $\square$ ),  $4$  ( $+$ ),  $5$  ( $\circ$ ),  $6$  ( $\diamond$ ).

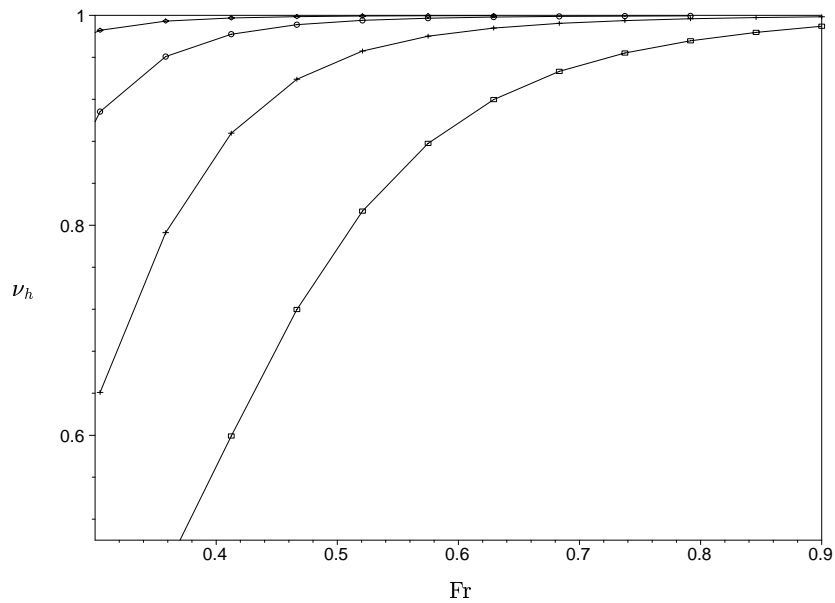


**Figure 4:** Wave attenuation per wavelength,  $\nu_h = \exp(\Re(\theta_1) \lambda_h)$ , versus the Froude number for mesh-width  $h = 2^{-l}$ ,  $l = 3$  ( $\square$ ),  $4$  ( $+$ ),  $5$  ( $\circ$ ),  $6$  ( $\diamond$ ).

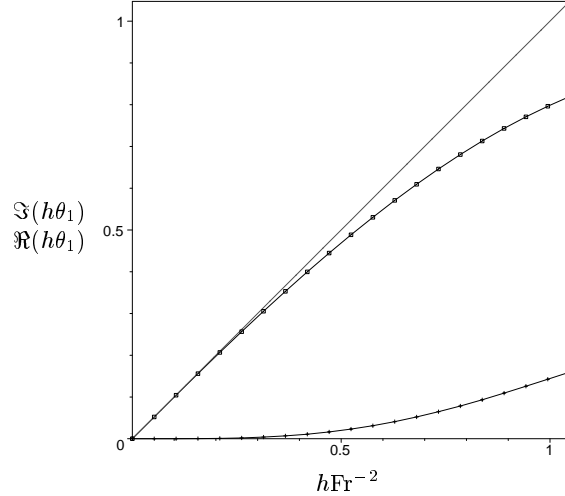


**Figure 5:**  $\Im(h\theta_1)$  ( $\square$ ) and  $\Re(h\theta_1)$  ( $+$ ) versus  $hFr^{-2}$ , according to dispersion relation (5.29).

Inspection reveals that for  $\theta \in \mathcal{H}^+$  equation (5.29) can be regarded as a relation between  $h\theta$  and  $hFr^{-2}$ . Hence, by (5.30), we have a relation between the non-dimensionalized wavenumbers, scaled with respect to the mesh-width, of stationary wave solutions of the continuous equations and of the discrete equations. Figure 5 displays the relation between  $h\theta_1$  and  $hFr^{-2}$  for  $\tau = 0$ .

## 6. SOLUTION

In `parnax`, the system of non-linear equations resulting from the discretization of the incompressible reduced Navier Stokes equations and the corresponding boundary conditions on a logically rectangular grid, is solved by a block Gauss-Seidel relaxation method. Moreover, nested iteration is employed to obtain an initial estimate. In this section we describe in detail the solution method and we investigate the computational complexity. Furthermore, we explain the incorporation of the iterative procedure for solving the free surface geometry.

### 6.1 Block Gauss-Seidel relaxation

The objective is to solve the system of non-linear equations (5.2), augmented with the discretized boundary conditions. Let  $\mathcal{V}_h$  denote the grid-nodes in the interior of  $\mathcal{V}$  and let  $\partial\mathcal{V}_h$  be a set of nodes associated with the boundary of the domain. For each  $\mathbf{i} \in \mathcal{V}_h \cup \partial\mathcal{V}_h$ , we write the equations to be solved as:

$$\mathbf{R}_i(\mathbf{v}_h, \varphi_h) = 0, \quad \mathbf{i} \in \mathcal{V}_h \cup \partial\mathcal{V}_h. \quad (6.1)$$

Equations (6.1) are called the residual equations. Hence, the aim is to find  $\mathbf{v}_h, \varphi_h$  such that the residual equations are solved for all nodes in  $\mathcal{V}_h \cup \partial\mathcal{V}_h$ .

We suppose that the grid-nodes are numbered such that  $\mathcal{V}_h \cup \partial\mathcal{V}_h = [0, 1, \dots, N_1] \times [0, 1, \dots, N_2]$ . The block Gauss-Seidel relaxation method implemented in `parnax` for solving (6.1) reads

**Algorithm:** *Block Gauss-Seidel relaxation*

```

initialize  $\varphi_h := \varphi_h^0, \mathbf{v}_h := \mathbf{v}_h^0$ 
while ( $\|\mathbf{R}_i(\mathbf{v}_h, \varphi_h)\|_{\mathcal{V}_h \cup \partial\mathcal{V}_h} > \epsilon$ ) {
  store  $\varphi_h^* := \varphi_h$ 

```

```

for ( $i_1 = 0, 1, 2, \dots, N_1$ ) {
  solve and update  $\mathbf{v}_h(\mathbf{i}), \varphi_h(\mathbf{i})$  from:  $\forall i_2 \mathbf{R}_i(\mathbf{v}_h, \varphi_h) = 0$ 
}
for ( $i_1 = N_1 - 1, N_1 - 2, \dots, 0$ ) {
   $\forall i_2$  update  $\varphi_h(\mathbf{i}) := \varphi_h^*(\mathbf{i}) + \omega(\varphi_h(\mathbf{i}) - \varphi_h^*(\mathbf{i})) + (1 - \omega)(\varphi_h(\mathbf{i} + \mathbf{e}_1) - \varphi_h^*(\mathbf{i} + \mathbf{e}_1))$ 
}
}

```

where  $\|\cdot\|_{\mathcal{V}_h \cup \partial\mathcal{V}_h}$  denotes some suitable norm. Note that the residual equations are first scanned in the direction in which the diffusive contribution to the momentum equations has been discarded. Next, the equations are scanned in the opposite direction, however, then only the pressure variable is modified. In the second step the residual equations corresponding to  $i_1$  are not actually solved, but the corrections computed in the first step are distributed.

Apart from the second step, the aforementioned method is identical to the algorithm described in [25]. There, it is shown that the contraction number (see, e.g., [12, p.98]) of the iteration is

$$\zeta \sim 1 - C \left(\frac{h}{L_2}\right)^2 \left(\frac{L_1}{L_2}\right)^2, \quad (6.2)$$

with  $C$  a constant of order one,  $h$  the mesh-width in the 1-direction and  $L_1$  and  $L_2$  the length of the computational domain in the 1- and 2-direction, respectively; see also [10, pp.307-313]. In [18] the convergence rate of the above algorithm is examined by means of Fourier analysis. It is established that slowest convergence occurs for low-wavenumber errors in the direction normal to the relaxation direction. The convergence rate of these critical modes is proportional to  $1 - O(h^2)$ .

These results imply that the method is convergent, but that the rate of convergence of the iteration deteriorates in such a manner that for  $h \rightarrow 0$  the amount of work per unknown, needed to reduce the initial error by a fixed factor, is  $O(h^{-2})$ . Usually, the objective is to reduce the evaluation error to the order of the discretization error. Supposing that the initial error is  $O(1)$ , one can show that in this case the amount of work required is  $O(h^{-2} |\log h|)$ . We conjecture that this asymptotic behavior of the computational complexity is unchanged by the second step.

### 6.2 Nested Iteration

Nested iteration is used to accelerate the computation. Using nested iteration, the initial guess is obtained by interpolation of the solution from a coarser grid. The initial guess on this coarse grid in turn is interpolated from an even coarser grid. This process is repeated recursively, until a grid is reached at which the problem can be solved at negligible computational expense.

Let the sequence of grids be numbered from coarsest to finest as  $l = 0, 1, \dots, L$ . Furthermore, let  $\mathbf{v}_l$  and  $\varphi_l$  denote grid functions on  $\mathcal{V}_l \cup \partial\mathcal{V}_l$  and let the level  $l$  problem be defined by:

$$\mathbf{R}_i^l(\mathbf{v}_l, \varphi_l) = 0, \quad \mathbf{i} \in \mathcal{V}_l \cup \partial\mathcal{V}_l. \quad (6.3)$$

The nested iteration algorithm reads:

**Algorithm:** *Nested iteration*

```

initialize  $\varphi_0 := \varphi_0^0, \mathbf{v}_0 := \mathbf{v}_0^0$ 
solve  $\mathbf{R}_i^0(\mathbf{v}_0, \varphi_0) = 0 \quad \mathbf{i} \in \mathcal{V}_0 \cup \partial\mathcal{V}_0$ 
for ( $l = 1, 2, \dots, L$ ) {
  initialize  $\varphi_l^0 := P_{l-1}^l \varphi_{l-1}, \mathbf{v}_l^0 := P_{l-1}^l \mathbf{v}_{l-1}$ 
  solve  $\mathbf{R}_i^l(\mathbf{v}_l, \varphi_l) = 0 \quad \mathbf{i} \in \mathcal{V}_l \cup \partial\mathcal{V}_l$ 
}

```

Here  $P_{l-1}^l$  stands for a sufficiently high order interpolation from level  $l - 1$  to level  $l$ .

Let  $p$  denote the order of consistency of the discretization. If the initial estimate for the level  $l$  problem contains an error of  $O(2^p h_l^p)$ , which can be accomplished if the usual mesh-width ratio of 2 between levels is employed and the interpolation is  $O(h^p)$  accurate, then  $O(h_l^{-2})$  Gauss-Seidel iterations are required to reduce the error to the order of the discretization error. The number of operations on level  $l - 1$  per level  $l$  node is then  $O(2^{-(p+3)} h_l^{-2})$ , which is only a small fraction of the work performed on level  $l$ . Hence, we can estimate the computational complexity of the nested iteration algorithm with block Gauss-Seidel iteration by the number of operations expended on the finest level when the initial estimate contains an error  $O(2^p h_L^p)$ , and ignore the costs of determining this initial estimate. Thus, the computational complexity of the algorithm is  $O(h_L^{-2})$ . This implies that the nested iteration removes the  $|\log(h)|$  dependence of the Gauss-Seidel relaxation and indeed accelerates convergence. However, this factor is small in comparison with the remaining  $h^{-2}$  dependence.

### 6.3 Free surface iteration

To solve the steady free-surface flow problem, we solve a sequence of sub-problems corresponding to the steady Navier-Stokes equations with the quasi free-surface condition imposed at an approximation to the steady free-surface. After each sub-problem evaluation, the free-surface is relocated, using the computed solution. Next, remeshing takes place, so that the mesh coincides with the newly computed shape of the domain. Finally, the results on the previous grid are transferred to the adapted grid to generate an initial estimate and the process is repeated.

The residual equations at the nodes associated with the free boundary follow from the discretized boundary conditions

$$\mathbf{B}_h(\mathbf{v}_h, \varphi_h) = \begin{pmatrix} K_h(\mathbf{v}_h, \varphi_h) \\ \mathbf{t}_h \cdot \boldsymbol{\tau}_h(\mathbf{v}_h) \cdot \mathbf{n}_h \end{pmatrix} = 0 \quad \mathbf{i} \in \partial\mathcal{S}_h, \quad (6.4)$$

where the operator  $K_h$  corresponds to the quasi free-surface condition and  $\mathbf{n}_h, \mathbf{t}_h$  are discrete approximations to the normal and tangential unit vectors to  $\mathcal{S}$ , respectively.

After each sub-problem evaluation, the wave-elevation at the sub-domain vertices is determined by

$$\eta_h(\mathbf{i} + \frac{1}{2}\mathbf{e}_1) = \text{Fr}^2 \left( \frac{1}{2}\varphi_{\mathbf{i} + \frac{1}{2}\mathbf{e}_2} + \frac{1}{2}\varphi_{\mathbf{i} + \mathbf{e}_1 + \frac{1}{2}\mathbf{e}_2} \right), \quad (6.5)$$

with  $\varphi_{\mathbf{i} + \frac{1}{2}\mathbf{e}_2}$  defined by (4.14). Subsequently, the nodes of the mesh are relocated, so that the resulting mesh coincides with the newly computed geometry of the domain. Let  $\mathbf{x}_h(\mathbf{j})$  be the sub-domain vertices and  $\bar{\mathbf{x}}_h(\mathbf{j})$  the sub-domain vertices of the adapted grid. We suppose that the remeshing is accomplished through a mapping:

$$\bar{\mathbf{x}}_h = \mathcal{M}(\eta_h, \mathbf{x}_h). \quad (6.6)$$

For example,  $\mathcal{M}$  can prescribe relative vertical stretching

$$\bar{x}_h^1(\mathbf{j}) = x_h^1(\mathbf{j}) \quad (6.7a)$$

$$\bar{x}_h^2(\mathbf{j}) = x_h^2(\mathbf{j}) + \frac{x_h^2(j^1, j^2) - x_h^2(j^1, 0)}{x_h^2(j^1, N^2) - x_h^2(j^1, 0)} (\eta(j^1) - x_h^2(j^1, N^2)), \quad (6.7b)$$

where we assume that the vertices are numbered such that  $x_h^2(j^1, 0)$  are associated with the bottom boundary and  $x_h^2(j^1, N^2)$  with the free-surface boundary.

The solution can be transferred from the cell-centers of the grid to the cell-centers of the modified grid by straightforward polynomial interpolation, e.g., a  $p$ -order interpolation:

$$\bar{\phi}_h(\mathbf{i}) = \sum_{\alpha=0}^{p-1} \phi_h(\mathbf{i} - \alpha\mathbf{e}_2) \prod_{\substack{\beta \neq \alpha \\ \beta=0}}^{p-1} \frac{\bar{y}_h^2(\mathbf{i}) - y_h^2(\mathbf{i} - \beta\mathbf{e}_2)}{y_h^2(\mathbf{i} - \alpha\mathbf{e}_2) - y_h^2(\mathbf{i} - \beta\mathbf{e}_2)} \quad (6.8)$$

with  $\mathbf{y}_h(\mathbf{i})$  the cell-centers,  $\bar{\mathbf{y}}_h(\mathbf{i})$  the cell-centers of the modified grid,  $\phi_h(\mathbf{i})$  a solution component in cell-center  $\mathbf{y}_h(\mathbf{i})$  and  $\bar{\phi}_h(\mathbf{i})$  the same component in the modified center  $\bar{\mathbf{y}}_h(\mathbf{i})$ . In general, it will be necessary to use multi-dimensional interpolation and the transfer can be described by

$$\bar{\phi}_h(\mathbf{i}) = \sum_{\mathbf{j} \in \mathcal{V}_h \cup \partial\mathcal{V}_h} a_{ij} \phi_h(\mathbf{j}) \quad (6.9)$$

The interpolation weights,  $a_{ij}$ , depend on the position of the cell-centers of the modified grid relative to the cell-centers of the original grid. Usually, the interpolation operation is local and  $a_{ij}$  is zero for all  $\mathbf{j}$  except some  $\mathbf{j}$  close to  $\mathbf{i}$ .

The entire iterative procedure can be summarized as:

**Algorithm:** *Free surface iteration*  
initialize  $\eta_h := \eta_h^0, \mathbf{x}_h := \mathcal{M}(\eta_h^0, \mathbf{x}_h^0), \varphi_h := \varphi_h^0, \mathbf{v}_h := \mathbf{v}_h^0$   
compute cell centers  $\{\mathbf{y}_h\}$   
solve  $\mathbf{R}_i(\mathbf{v}_h, \varphi_h) = 0 \quad \mathbf{i} \in \mathcal{V}_h \cup \partial\mathcal{V}_h$   
while ( $\|\text{Fr}^2 \varphi_h(\mathbf{i}) - \eta_h(\mathbf{i})\|_{\mathcal{S}_h} > \epsilon$ ) {  
  compute wave-elevation,  $\eta_h$ , from (6.5)  
  remesh:  $\bar{\mathbf{x}}_h := \mathcal{M}(\eta_h, \mathbf{x}_h)$   
  compute cell centers  $\{\bar{\mathbf{y}}_h\}$   
  transfer solution:  $(\mathbf{v}_h, \varphi_h)(\mathbf{i}) := \sum a_{ij}(\mathbf{v}_h, \varphi_h)(\mathbf{j})$   
  update  $\mathbf{x}_h := \bar{\mathbf{x}}_h, \mathbf{y}_h := \bar{\mathbf{y}}_h$   
  solve  $\mathbf{R}_i(\mathbf{v}_h, \varphi_h) = 0 \quad \mathbf{i} \in \mathcal{V}_h \cup \partial\mathcal{V}_h$   
}

If the residual equations are solved with an iterative solver, the result contains 3 different main errors. Firstly, an error is present because the residual equations are not solved exactly. We call this error the evaluation error,  $\epsilon$ . Secondly, an error occurs due to the fact that the domain on which the computation is performed, is only an approximation of the domain corresponding to the actual free-boundary position. We call this error the domain error,  $\epsilon_V$ . Thirdly, the result contains a discretization error,  $e_h$ . Therefore, in the above algorithm, the residual equations only have to be solved approximately. It is sufficient to reduce the evaluation error such that  $\epsilon \leq \epsilon_V + e_h$ , because a further reduction does not essentially improve the result.

The iterative procedure for the free-surface can be incorporated in the block Gauss-Seidel method with nested iteration in a straightforward manner: The problem to be solved on level  $l$  is defined to be the steady free-surface problem on the level  $l$  grid. The residual equations are solved by means of the block Gauss-Seidel relaxation. However, on coarse grids in the nested iteration algorithm, the discretization error can be much larger than the domain error. Because displacing the free surface on such a coarse grid does not essentially improve the solution, it is then useful to proceed to the next finer grid without making any free-surface adjustments.

We consider the computational complexity of the free-surface iteration. The expense of solving the sub-problems by an iterative solver decreases during the free surface iteration, because an increasingly accurate initial estimate can be obtained from the interpolation of the previous solution. We define the contraction number of the free-surface iteration by

$$\zeta \equiv \|p_h^{n+1}(\mathbf{i})\|_{\mathcal{S}_h^{n+1}} / \|p_h^n(\mathbf{i})\|_{\mathcal{S}_h^n}. \quad (6.10)$$

with  $p_h^n(\mathbf{i})$  the pressure after  $n$  iterations. Because a converged solution is reached if the pressure at the free surface vanishes, we refer to  $\|p_h(\mathbf{i})\|_{\mathcal{S}_h}$  as the *pressure defect*. Assuming that the disturbance induced by displacing the boundary is proportional to the displacement and, by (6.5), to the pressure defect, we infer that the amount of work that is required between consecutive iterations contracts with  $\zeta$  as well. Hence, denoting by  $W$  the computational work invested in solving the first sub-problem

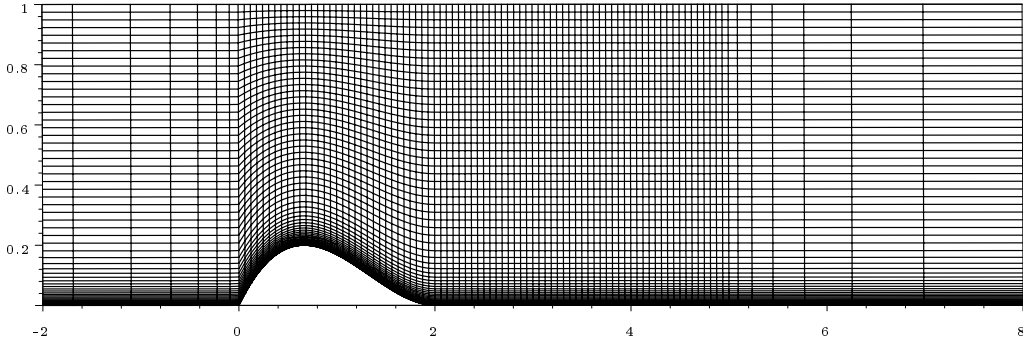


**Figure 6:** Typical example of a grid used in the numerical experiments ( $h = 2^{-4}$ ).

and by  $w$  the incremental work involved in obtaining the solution to the second sub-problem, the cumulative computational expense of solving the  $N$ -th sub-problem is:

$$W + \sum_{\alpha=0}^{N-1} \zeta^\alpha w = W + w \frac{\zeta^N - 1}{\zeta - 1} \leq W + \frac{w}{1 - \zeta}. \quad (6.11)$$

Generally, one may expect that  $w$  is already much smaller than  $W$ . Therefore, for modest values of the contraction number, the cost of solving the free-surface problem is essentially determined by the expense of the first sub-problem, regardless of the accuracy required. Consequently, for small  $\zeta$ , the computational complexity of the free-surface flow problem is similar to that of a fixed domain problem.

Observe that the contraction number of the free-surface iteration (6.10) does not depend on the mesh-width of the grid. Hence, we anticipate mesh-width independent convergence behavior of the iterative method for the free-surface.

## 7. NUMERICAL EXPERIMENTS & RESULTS

To test the algorithm described in Section 6.3 and to verify the results of the analysis presented in Section 5, we conducted numerical experiments for subcritical flow over an obstacle in a channel at  $Fr = 0.43$  and  $Re = 1.5 \times 10^5$ , with both parameters scaled with respect to the entrance velocity at the free surface and the channel depth. An algebraic turbulence model was employed. The geometry of the obstacle is described in [5]. We considered obstacles with a non-dimensionalized height  $E = 0.15$  and  $E = 0.20$ . The first test case displays small amplitude waves that exhibit behavior in accordance with linear wave theory. This test case serves to verify the results of the analysis presented in Section 5. The second test case is in accordance with the experimental setup in [5] and displays large amplitude waves that exhibit typical non-linear behavior, e.g., acute wave-crest angles and wavelength contraction.

The experiments were performed on different grids with horizontal mesh-widths  $h = 2^{-l}$ ,  $l = 3, \dots, 6$ . In each case, the number of grid cells in the vertical direction was 70 and exponential grid-stretching was applied to resolve the boundary layer at the bottom. Furthermore, the grid was exponentially stretched in the horizontal direction towards the lateral boundaries to reduce reflections. A typical example of a grid used in the numerical experiments is presented in Figure 6.

To further reduce reflections from lateral boundaries, artificial damping was introduced in the vicinity of the lateral boundaries by inserting a second order derivative into the quasi free surface

$n$	$\ p^n\ _S$			
	case I, $l = 5$	case I, $l = 6$	case II, $l = 5$	case II, $l = 6$
0	$6.42^{-3}$	$6.81^{-3}$	$1.27^{-2}$	$1.36^{-2}$
1	$2.01^{-3}$	$1.83^{-3}$	$7.09^{-3}$	$7.51^{-3}$
2	$2.51^{-4}$	$2.97^{-4}$	$3.13^{-3}$	$3.96^{-3}$
3	$3.42^{-5}$	$5.21^{-5}$	$8.96^{-4}$	$1.41^{-3}$
4	$4.16^{-6}$	$4.18^{-6}$	$4.71^{-4}$	$8.46^{-4}$
5	$3.79^{-7}$	$7.75^{-7}$	$2.31^{-4}$	$5.21^{-4}$
6	$1.39^{-7}$	$1.39^{-7}$	$1.07^{-4}$	$3.32^{-4}$
7	$1.45^{-7}$	$8.63^{-8}$	$4.31^{-5}$	$2.13^{-4}$
8	$6.34^{-8}$	$8.77^{-8}$	$1.55^{-5}$	$1.37^{-4}$
9	$4.30^{-8}$	$8.07^{-8}$	$6.74^{-6}$	$8.71^{-5}$
10	$3.03^{-8}$	$6.97^{-8}$	$3.98^{-6}$	$5.66^{-5}$

**Table 1:** Pressure defect at the free surface after consecutive iterations for test-case I,  $l = 5, 6$  and test-case II,  $l = 5, 6$ .

condition, i.e., the quasi free-surface condition was replaced by

$$v_1 \frac{\partial \varphi}{\partial x_1} + v_2 \frac{\partial \varphi}{\partial x_2} - \text{Fr}^{-2} v_2 - \mu(x_1) \frac{\partial^2 \varphi}{\partial x_1^2} = 0, \quad (7.1)$$

with  $\mu(x_1)$  a function that vanishes in the interval  $x_1 \in [-2, 4]$  and increases towards the lateral boundaries.

Direct solution of the sub-problems with a second order discretization of the quasi free-surface condition by means of the block Gauss-Seidel relaxation proved fragile. Therefore, the second order discretized problems were solved by means of defect correction, with the sub-problems with first order discretization of the quasi free-surface condition serving as approximate operator.

After each sub-problem evaluation, the grid was adapted using the relative vertical stretching (6.7) and an initial estimate on the adapted grid was generated by interpolation from the solution on the previous grid according to (6.8), with interpolation order  $p = 4$ .

### 7.1 Test-case I

To examine the convergence behavior of the iterative method for solving the free-surface Navier-Stokes problem, we monitored the of the pressure defect at the free-surface after consecutive sub-problem evaluations and updates of the free-surface position, defined by  $\|p^n\|_S = \sum_j h_j |p_j| / \sum_k h_k$ , with  $n = 0, 1, 2, \dots$  the iteration number. Table 1 lists the results for the grids with horizontal mesh-width  $h^l$ ,  $l = 5, 6$ . In Figure 7 the pressure is plotted versus the iteration number. The results confirm convergence of the method, with an average contraction number  $\zeta \approx 0.14$  for  $l = 5$  and  $\zeta = 0.16$  for  $l = 6$ . Indeed, the contraction number appears to be essentially independent of the mesh-width. After several iterations the contraction number increases. However, this is entirely due to the fact that the sub-problems are solved only by approximation. If the tolerance on the residual of the sub-problems is reduced, i.e. if the sub-problems are solved more accurately, then the original contraction number is recovered.

Figure 8 displays the computed wave-elevation on grids with horizontal mesh-widths  $h = 2^{-l}$ ,  $l = 3, \dots, 6$ . The corresponding wavelength and wave-attenuation are compared to the predictions according to discrete dispersion relation (5.26) in Table 2. For the wave attenuation, the numerical

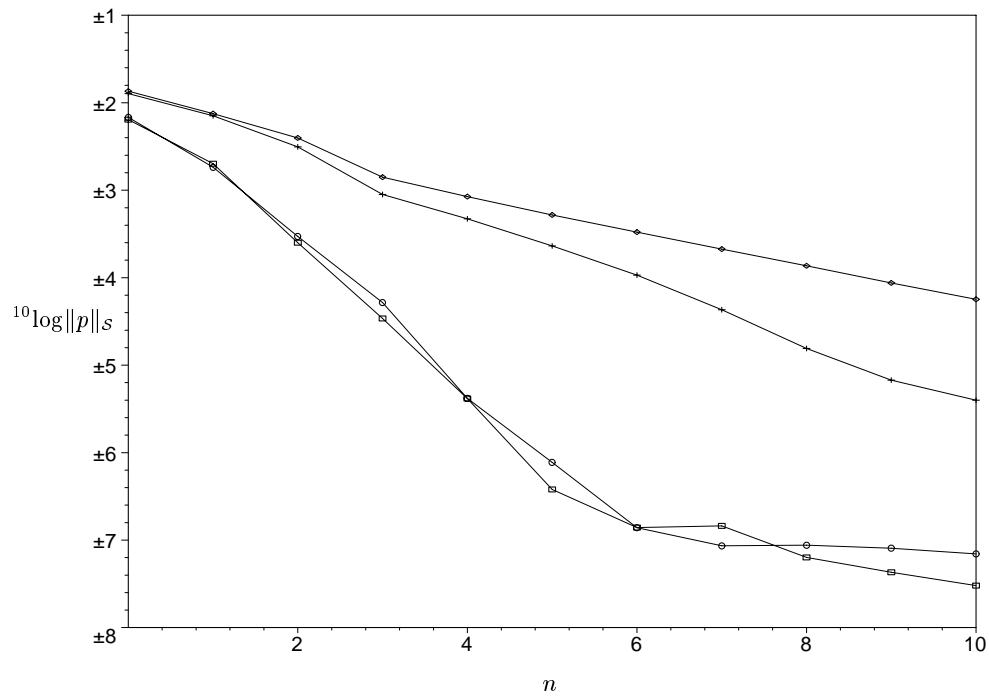


**Figure 7:** Pressure defect at the free surface versus the iteration number for test-case I,  $l = 5$  ( $\square$ ),  $l = 6$  ( $\circ$ ) and test-case II  $l = 5$  ( $+$ ),  $l = 6$  ( $\diamond$ ).

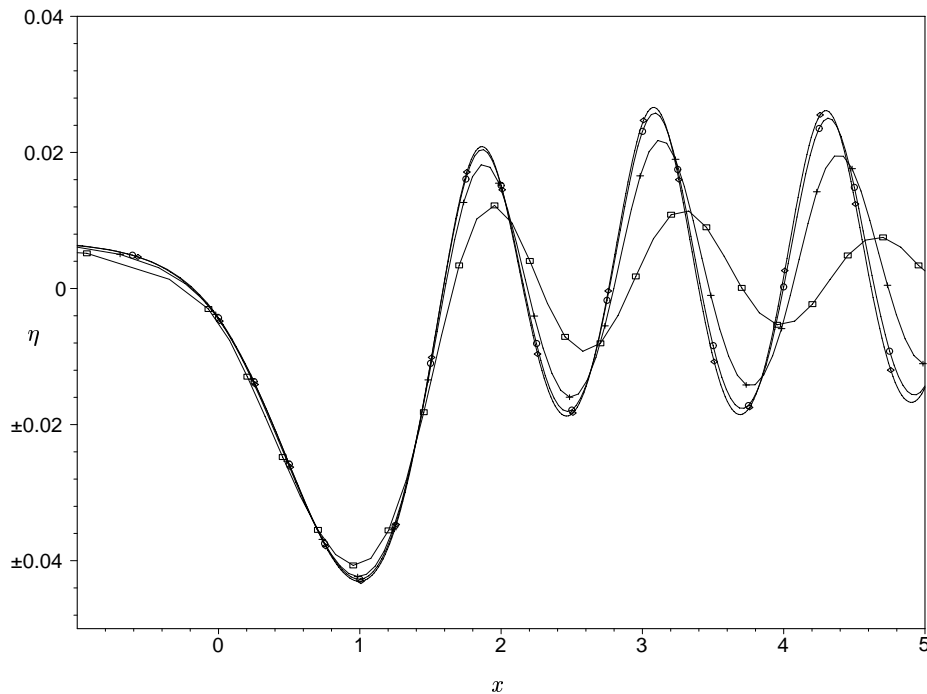


**Figure 8:** Computed wave elevation for test-case I on grids with mesh-widths  $h = 2^{-l}$ ,  $l = 3$  ( $\square$ ),  $4$  ( $+$ ),  $5$  ( $\circ$ ),  $6$  ( $\diamond$ ).

results and the predictions exhibit good agreement. The results for the wavelength display a marked difference. This can be explained by the fact that the wavelength is sensitive to Froude-number deviations incurred by, e.g., non-uniformity of the inlet-velocity profile. More important, however, is the fact that (5.26) accurately predicts the discretization error in the wavelength of the computed results.

### 7.2 Test-case II

To examine the convergence of the iterative method for the second test case, we again monitored the pressure defect at the free surface. For  $l = 5, 6$ , the results are listed in Table 1 and plotted in Figure 7. The pressure defect vanishes with an average contraction number  $\zeta \approx 0.45$  for  $l = 5$  and  $\zeta = 0.52$  for  $l = 6$ . The significant mesh-width dependence of the contraction number can be ascribed to a substantial difference between the solutions on the grids with  $l = 5$  and  $l = 6$ . Mesh-width independence of the contraction number is achieved only asymptotically for vanishing mesh-width. Due to the strong non-linearity, this asymptotic behavior is not yet apparent. Moreover, the strong non-linearity causes a deterioration in convergence behavior, in comparison with test case I. Figure 9 illustrates the convergence of the wave elevation.

In Figure 10, the computed wave elevation is compared with measurements from [5]. In [5], a non-dimensionalized wavelength  $\lambda = 1.10 \pm 10\%$  and amplitude  $a = 4.5 \times 10^{-2} \pm 15\%$  are reported for the trailing wave. The trailing wave of the computed wave elevation on the grid with  $l = 6$  displays wavelength  $\lambda = 1.11$  and amplitude  $a = 6.5 \times 10^{-2}$ . Clearly, the computed wavelength agrees well with the measurements. The amplitude is, however, slightly overestimated.

$l$	wavelength		attenuation	
	comput.	analysis	comput.	analysis
3	1.37	1.33	0.63	0.64
4	1.27	1.21	0.90	0.91
5	1.23	1.17	0.98	0.99
6	1.22	1.16	0.99	1.00

**Table 2:** Wavelength and wave attenuation of the numerical results and by dispersion relation (5.26) for  $h = 2^{-l}$ ,  $l = 3, \dots, 6$ .

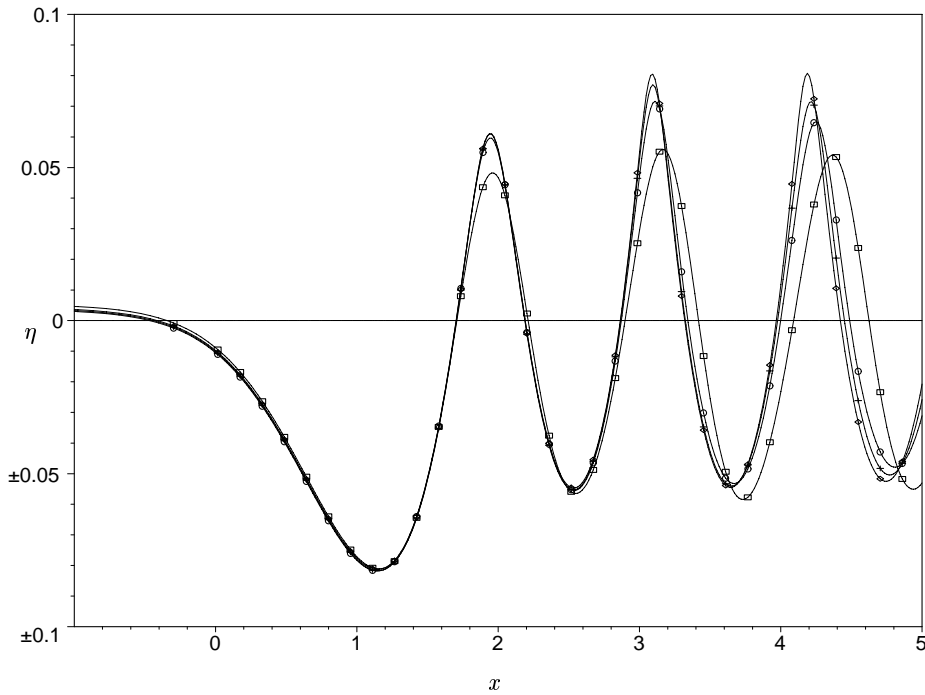


**Figure 9:** Wave elevation for  $l = 6$  after  $n$  iterations:  $n = 0$  (none),  $n = 1$  ( $\square$ ),  $n = 3$  ( $\circ$ ),  $n = 5$  ( $+$ ), final ( $\diamond$ ).

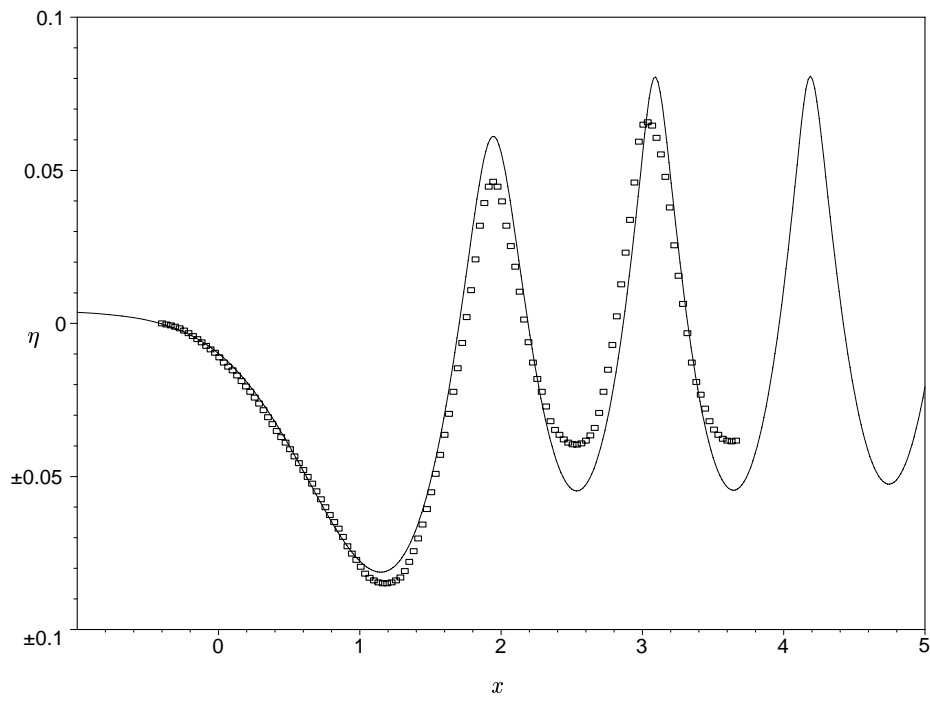


**Figure 10:** Computed wave elevation for  $l = 6$  (solid line) and measurements from [5] (markers only).

## 8. CONCLUSIONS

Motivated by the demand for more efficient computational methods for steady free-surface Navier-Stokes flow in practical applications, we propose a new iterative solution method. The method solves a sequence of sub-problems, with a quasi free-surface condition imposed at the free surface. After each sub-problem evaluation, an improved approximation to the free-surface location is obtained. The method can be formulated in the framework of optimal shape design methods. This formulation reveals that the method relies on the quasi free-surface condition to ensure that the disturbance induced by the displacement of the boundary is small. The update obtained from the normal dynamic condition is a descent direction and, therefore, convergence is ensured, provided that the flow is sufficiently smooth.

We considered the discretization of the reduced incompressible Navier-Stokes equations implemented in `parmax` and discussed discretization of the quasi free-surface condition. We then analyzed the properties of the discrete equations. Dispersion relations were derived for the semi-discrete equations corresponding to the free-surface flow problem in a channel of unit depth and of infinite depth.

We discussed the block Gauss-Seidel iteration and the nested iteration algorithm used in `parmax`. Analysis of the computational complexity showed that for horizontal mesh-width  $h \rightarrow 0$ , the rate of convergence of the method is  $1 - O(h^2)$ . We then considered the free-surface iteration. We showed that the convergence behavior of the iteration is mesh-width independent. Moreover, if the sub-problems are solved by an iterative solver and a sufficiently small contraction number for the free-surface iteration can be realized, the computational cost of the free-surface problem is similar to that of a fixed domain problem.

Numerical results were presented for flow over a protuberance in a channel of unit depth. The results show good agreement with measurements and with the predictions of the discrete dispersion relation. Furthermore, for the test-case presented, the results confirm that the convergence behavior of the free-surface iteration is essentially mesh-width independent. Even for a strongly non-linear test-case a reasonable contraction number for the free-surface iteration is realized and the computational complexity of the free-surface flow problem is only marginally higher than that of a comparable fixed domain problem. The results indicate that the new iterative method is indeed suitable for the efficient solution of steady free-surface Navier-Stokes flow problems.

## 9. RECOMMENDATIONS FOR FUTURE RESEARCH

- The optimal shape design formulation of the problem indicates that the applicability of the iterative method in its current form is restricted to smooth flows. However, it also reveals that this restriction can be dissolved by introducing a more accurate approximation of the pressure gradient in the quasi free-surface condition and the surface update. Different test-cases should be initiated to establish the limitations of the method in its present form and to investigate the improvement introduced by a more accurate approximation of the pressure gradient.
- The response of the method to surface penetrating objects should be investigated. In 2D, a suitable test-case to do so, is the transom stern flow problem, discussed in, e.g., [14, 29]. Alternatively, flow around surface penetrating objects in 3D can be investigated.
- The dispersion relations provide a means to develop discretization schemes with specific properties, e.g., low numerical damping. Discretization schemes with favorable properties should be determined and tested.
- The transition region that is currently employed in the computations to reduce reflections from lateral boundaries is computationally inefficient and sensitive to parameter variations, such as grid-stretching. Moreover, it appears that the complexity of the computational problem, i.e., the performance of the iterative solver, depends on the type of lateral boundary conditions employed. The dispersion relations and the theory developed in [8] can serve in the development

of suitable highly absorbing lateral boundary conditions for the free-surface flow problem. A further attempt should be made to derive such highly absorbing boundary conditions.

## References

1. R. Aris. *Vectors, Tensors and the Basic Equations of Fluid Mechanics*. Prentice-Hall, Englewood Cliffs, N.J., 1962.
2. K. Böhmer, P.W. Hemker, and H.J. Stetter. The defect correction approach. *Computing*, Suppl. 5:1–32, 1984.
3. A. Brandt and N. Dinar. Multigrid solution to elliptic flow problems. In *Numerical Methods in PDE*, pages 53–147. Academic Press, New York, 1977.
4. H. van Brummelen. Analysis of the incompressible Navier-Stokes equations with a quasi free-surface condition. Technical report, CWI, 1999. Available at <http://www.cwi.nl/static/publications/reports/MAS-1999.html>.
5. J. Cahouet. *Etude Numérique et Experimentale du Problème Bidimensionnel de la Résistance de Vagues Non-Linéaire*. PhD thesis, ENSTA, Paris, 1984. (In French).
6. C.W. Dawson. A practical computer method for solving ship-wave problems. In *Proceedings 2nd International Conference on Numerical Ship Hydrodynamics*, pages 30–38, Berkeley, 1977.
7. J.H. Ellison, C.A. Hall, and T.A. Porsching. An unconditionally stable convergent finite difference method for Navier-Stokes problems on curved domains. *SIAM J. Numer. Anal.*, 6:1233–1248, 1987.
8. B. Engquist and A. Majda. Absorbing boundary conditions for the numerical simulation of waves. *Math. Comp.*, 31:629–651, 1977.
9. J. Farmer, L. Martinelli, and A. Jameson. A fast multigrid method for solving the nonlinear ship wave problem with a free surface. In *Proceedings 6th International Conference on Numerical Ship Hydrodynamics*, Iowa 1993.
10. C.A.J. Fletcher. *Computational Techniques for Fluid Dynamics 2*. Springer Verlag, Berlin, 1988.
11. L. Fuchs and H.S. Zhao. Solution of three-dimensional viscous incompressible flow by a mutli-grid method. *Int. J. Num. Meth. Fluids*, 4:539–555, 1984.
12. W. Hackbusch. *Multi-Grid Methods and Applications*. Springer Verlag, Berlin, 1985.
13. F.H. Harlow and J.E. Welch. Numerical calculation of time-dependent viscous incompressible flow of fluid with free-surface. *Phys. of Fluids*, 8:2182–2189, 1965.
14. H.J. Haussling. Two-dimensional linear and nonlinear stern waves. *J. Fluid Mech.*, 97:759–769, 1980.

15. C.W. Hirt and B.D. Nichols. Volume of fluid (VOF) method for the dynamics of free boundaries. *J. Comput. Phys.*, 39:201–225, 1981.
16. M. Hoekstra. *Numerical Simulation of Ship Stern Flows with a Space-Marching Navier-Stokes Method*. PhD thesis, Delft University of Technology, Netherlands, 1999.
17. F.J. Kelecy and R.H. Pletcher. The development of a free surface capturing approach for multi-dimensional free surface flows in closed containers. *J. Comput. Phys.*, 138:939–980, 1997.
18. B. Koren. Note on PARNASSOS, a Navier-Stokes method for ship stern flows. Technical report, CWI, 1998. Available at <http://www.cwi.nl/static/publications/reports/MAS-1998.html>.
19. M.J. Lighthill. *Waves in Fluids*. Cambridge University Press, Cambridge, 1978.
20. M.J. Lighthill. *Introduction to Fourier Analysis and Generalised Functions*. Cambridge University Press, London, 1958.
21. W. Mulder, S. Osher, and J.A. Sethian. Computing interface motion in compressible gas dynamics. *J. Comput. Phys.*, 100:209–228, 1992.
22. O. Pironneau. *Optimal Shape Design for Elliptic Systems*. Springer Verlag, Berlin, 1984.
23. H. Raven and H. van Brummelen. A new approach to computing steady free-surface viscous flow problems. In *1<sup>st</sup> MARNET-CFD Workshop*, Barcelona, 1999. Available at [http://www.marin.nl/projects/cph\\_parnassos\\_720.html](http://www.marin.nl/projects/cph_parnassos_720.html).
24. H.C. Raven. *A Solution Method for the Nonlinear Ship Wave Resistance Problem*. PhD thesis, Delft University of Technology, Netherlands, 1996.
25. S.G. Rubin and D.R. Reddy. Analysis of global pressure relaxation for flows with strong interaction and separation. *Comput. Fluids*, 11:281–306, 1983.
26. L.E. Scriven. Dynamics of a fluid interface. *Chem. Eng. Sc.*, 12:98–108, 1960.
27. S. Ta’san. *Inverse Design and Optimization Methods*, volume 5 of *VKI Lecture Series*, chapter Theoretical Tools for Problem Setup. Von Karman Institute for Fluid Dynamics, 1997.
28. S. Ta’san. *Inverse Design and Optimization Methods*, volume 5 of *VKI Lecture Series*, chapter Introduction to Shape Design and Control. Von Karman Institute for Fluid Dynamics, 1997.
29. J.-M. Vanden-Broeck. Nonlinear stern waves. *J. Fluid. Mech.*, 96:603–611, 1980.